ARTICLES
https://doi.org/10.1038/s43018-020-0028-4

nature cancer

Check for updates

Extracellular cGAMP is a cancer-cell-produced immunotransmitter involved in radiation-induced anticancer immunity

Jacqueline A. Carozza[1,2,7], Volker Böhnert[2,3,7], Khanh C. Nguyen[4], Gemini Skariah[2,3], Kelsey E. Shaw[2,3], Jenifer A. Brown[2,5], Marjan Rafat[6], Rie von Eyben[6], Edward E. Graves[6], Jeffrey S. Glenn[4], Mark Smith[2] and Lingyin Li[2,3]✉

2′3′-Cyclic GMP-AMP (cGAMP) is an intracellular second messenger that is synthesized in response to cytosolic double-stranded DNA and activates the innate immune STING pathway. Our previous discovery of its extracellular hydrolase ENPP1 hinted at the existence of extracellular cGAMP. Here we detected that cGAMP is continuously exported but then efficiently cleared by ENPP1, explaining why it has previously escaped detection. By developing potent, specific and cell-impermeable ENPP1 inhibitors, we found that cancer cells continuously export cGAMP in culture at steady state and at higher levels when treated with ionizing radiation (IR). In mouse tumors, depletion of extracellular cGAMP decreased tumor-associated immune cell infiltration and abolished the curative effect of IR. Boosting extracellular cGAMP with ENPP1 inhibitors synergized with IR to delay tumor growth. In conclusion, extracellular cGAMP is an anticancer immunotransmitter that could be harnessed to treat cancers with low immunogenicity.

The second messenger cGAMP[1] has pivotal roles in anticancer and antiviral innate immunity. It is synthesized by the enzyme cyclic GMP-AMP synthase (cGAS)[2] in response to double-stranded DNA (dsDNA) in the cytosol, which is a danger signal for damaged or cancerous cells and intracellular pathogens[3–7]. cGAMP binds and activates its endoplasmic reticulum (ER) surface receptor stimulator of interferon genes (STING)[8] to activate production of type I interferons (IFNs). These potent cytokines trigger downstream innate and adaptive immune responses to clear the threat.

In addition to activating STING within its cell of origin, cGAMP can spread to bystander cells through gap junctions in epithelial cells[9]. This cell–cell communication mechanism alerts adjacent cells of the damaged cell and also, unfortunately, accounts for the spread of drug-induced liver toxicity[10,11] and brain metastases[12]. In addition, cytosolic cGAMP can be transmitted to other cells via viral particles[13,14]. In both transmission modes, cGAMP is not exposed to the extracellular space. Finally, tumor-derived cGAMP has been reported to activate STING in noncancer cells through unknown mechanisms and eventually activate natural killer (NK) cell responses[15].

cGAMP is synthesized in the cytosol and cannot passively cross the cell membrane, owing to its two negative charges. However, two pieces of evidence hinted that cGAMP is exported to the extracellular space to signal other cells. First, we identified a cGAMP hydrolase, ectonucleotide pyrophosphatase phosphodiesterase 1 (ENPP1)[16], which is the only detectable cGAMP hydrolase reported. Interestingly, ENPP1 is annotated as an extracellular enzyme, both as a membrane-bound form and as a soluble form in the serum[16]. Second, when added to cell medium or injected into tumors, cGAMP and its analogs can cross the cell membrane to activate STING in most cell types[17,18]. We and others subsequently identified a direct cGAMP importer, SLC19A1 (refs. [19,20]).

Here we report direct evidence for cGAMP export by cancer cells and the role of extracellular cGAMP in anticancer immune detection. We subsequently developed small-molecule inhibitors of ENPP1 with nanomolar potency and used them to boost extracellular cGAMP concentration, immune infiltration and tumor progression. Taking these findings together, we characterize cGAMP as an immunotransmitter that can be harnessed to treat cancer.

Results

cGAMP is exported from 293T cGAS *ENPP1*$^{-/-}$ cells as a soluble factor. To test the hypothesis that cGAMP is present extracellularly, we first developed a liquid chromatography tandem mass spectrometry (LC–MS/MS) method to quantify cGAMP at concentrations as low as 0.3 nM in cell media (extracellular) and cell extracts (intracellular) (Extended Data Fig. 1a–d)[21,22]. We chose to use 293T cells, which express undetectable amounts of cGAS and STING proteins[2,8,23] (Extended Data Fig. 1e). By stably expressing mouse cGAS and knocking out *ENPP1*, we created a 293T cGAS ENPP1^{low} cell line and then isolated a single clone to create a 293T cGAS *ENPP1*$^{-/-}$ cell line (Extended Data Fig. 1e). We also used serum-free medium because serum contains a soluble form of ENPP1 (ref. [24]). By using this ENPP1-free cell culture system, we detected basal low-micromolar intracellular cGAMP concentrations in 293T cGAS *ENPP1*$^{-/-}$ cells without any stimulation (Fig. 1a), but not in the parent 293T cells (Fig. 1b). This was surprising at first, but can now be explained by multiple reports showing

[1]Department of Chemistry, Stanford University, Stanford, CA, USA. [2]Stanford ChEM-H, Stanford University, Stanford, CA, USA. [3]Department of Biochemistry, Stanford University, School of Medicine, Stanford, CA, USA. [4]Departments of Medicine and Microbiology & Immunology, Stanford University, School of Medicine, Stanford, CA, USA. [5]Biophysics Program, Stanford University, Stanford, CA, USA. [6]Department of Radiation Oncology, Stanford University, School of Medicine, Stanford, CA, USA. [7]These authors contributed equally: Jacqueline A. Carozza, Volker Böhnert.
✉e-mail: lingyinl@stanford.edu

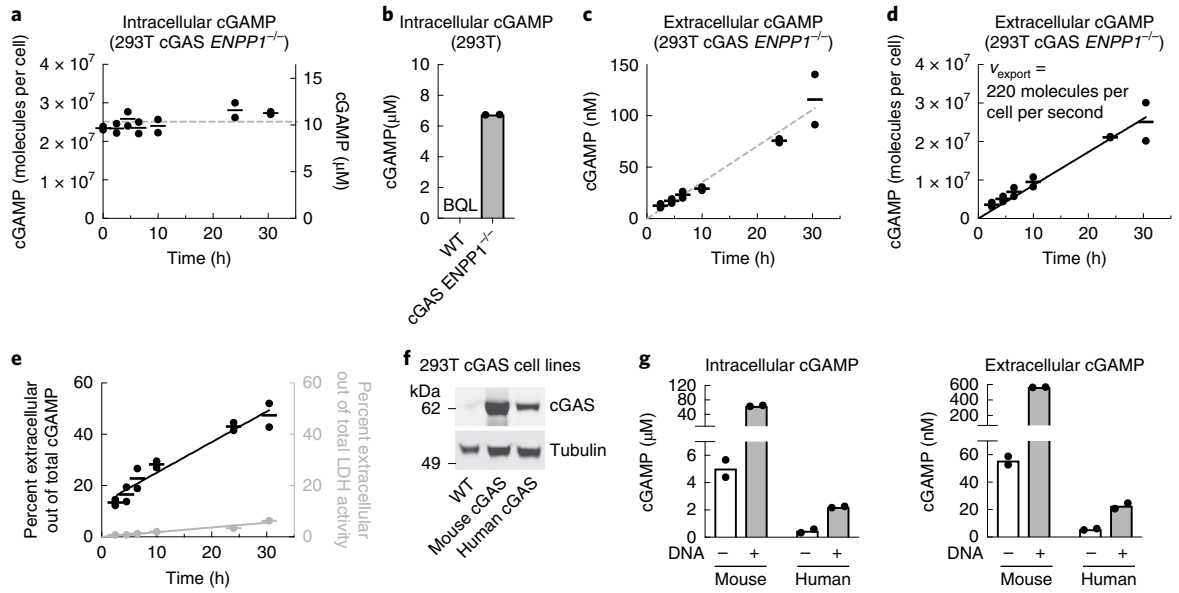

Fig. 1 | cGAMP is exported from 293T cGAS *ENPP1*$^{-/-}$ cells. a, Intracellular concentrations of cGAMP from 293T cGAS *ENPP1*$^{-/-}$ cells without exogenous stimulation. At time 0, cells were replenished with serum-free medium. The dashed line represents mean cGAMP concentration over all time points. Data are from one experiment, representative of three independent validations (Supplementary Fig. 1a,b); two cell culture replicates are plotted for each time point. **b**, Intracellular concentrations of cGAMP from WT 293T and 293T cGAS *ENPP1*$^{-/-}$ cells without exogenous stimulation at steady state. Data are from one experiment (supported by experiments in Fig. 2c and Supplementary Fig. 1c); two cell culture replicates are plotted. **c**, Extracellular concentrations of cGAMP from the experiment in **a**. The dashed line represents linear regression. Data and regression are from one experiment, representative of three independent validations (Supplementary Fig. 1a,b); two cell culture replicates are plotted for each time point. **d**, Linear regression of cGAMP exported per cell over time. Data were reanalyzed from the experiment in **a** and **c**. Linear regression is representative of regressions from three independent validations (Supplementary Fig. 1a,b). **e**, The fraction of extracellular out of total cGAMP molecules (left *y* axis; data reanalyzed from the experiment in **a** and **c**) compared to the fraction of extracellular out of total LDH activity as a proxy for cell death (right *y* axis). Data for the LDH assay are from one experiment, representative of four independent validations (Supplementary Fig. 1d–f); two cell culture replicates are plotted. Linear regressions were performed for the data shown. **f**, Expression of cGAS in WT 293T cells, 293T cells stably expressing mouse cGAS and 293T cells stably expressing human cGAS assessed by western blotting. Data are from one experiment (full scan of blot available as source data). **g**, Intracellular and extracellular concentrations of cGAMP for 293T cells stably expressing mouse cGAS and 293T cells stably expressing human cGAS. Cells were left untransfected or transfected with 0.5 μg ml^{-1} empty pcDNA6 vector. After 24 h, cells were refreshed with serum-free medium and incubated for another 24 h before measuring cGAMP. Data are from one experiment, representative of two independent validations (Supplementary Fig. 1g); two cell culture replicates are plotted. In **a**–**e** and **g**, cGAMP was measured by LC–MS/MS and replicates are plotted individually with a bar representing the mean. BQL, below the quantification limit.

that cancer cells harbor cytosolic dsDNA, the activator of cGAMP synthesis, as a result of erroneous DNA segregation[25–27]. After replenishing the cells with fresh medium, we measured a linear increase in extracellular cGAMP levels for up to 30 h (Fig. 1c). The amount of cGAMP exported was substantial given that, after 30 h, the number of cGAMP molecules outside the cells was equal to the number inside (Fig. 1d). We detected a negligible amount of cell death on the basis of extracellular lactose dehydrogenate (LDH) activity, suggesting that cGAMP in the medium is exported by live cells (Fig. 1e). We calculated the export rate (v_{export}) to be 220 molecules per cell per second (Fig. 1d). Finally, although human cGAS has been shown to be slower than its mouse counterpart[28], we measured both intracellular and extracellular cGAMP in human-cGAS-expressing 293T cells at steady state, which could be further induced by dsDNA transfection (Fig. 1f,g).

We have previously shown that there are multiple cGAMP importers, including the solute carrier SLC19A1 (refs. [19,20]). We postulate that there are also multiple cGAMP export mechanisms. To characterize the cGAMP export mechanism in 293T cells, we first determined whether cGAMP was enclosed in extracellular vesicles (as previously reported[13,14]) or freely soluble. We filtered conditioned medium from 293T cGAS *ENPP1*$^{-/-}$ cells through a 10-kDa MWCO filter, which retains extracellular vesicles and proteins. cGAMP passed through the filter, suggesting that it is exported as a freely soluble molecule (Fig. 2a). To further confirm that extracellular cGAMP exported by 293T cells is predominantly in a soluble form, we used CD14$^+$ human peripheral blood mononuclear cells (PBMCs) as a reporter. These cells have previously been shown to take up soluble cGAMP, which leads to IFN-β production[18,19]. We observed that CD14$^+$ PBMCs responded to submicromolar concentrations of soluble cGAMP by upregulating *IFNB1* (Extended Data Fig. 2a,b). Conditioned medium from DNA-transfected cGAS-expressing 293T cGAS ENPP1^{low} cells, but not DNA-transfected 293T cells, induced *IFNB1* expression in CD14$^+$ cells, suggesting that the activity is a result of extracellular cGAMP produced by 293T cells (Fig. 2b,c). Addition of purified soluble recombinant mouse ENPP1 (mENPP1) (Extended Data Fig. 2c) depleted detectable cGAMP in the conditioned medium and also ablated this activity (Fig. 2b,d). Because soluble ENPP1 (molecular weight of ~100 kDa) cannot permeate membranes and, thus, can only access soluble extracellular cGAMP, we conclude that 293T cells export soluble cGAMP.

We then determined the ATP dependence of the dominant cGAMP exporter in 293T cells. When we depleted ATP for 1 h, cell viability was not affected (Extended Data Fig. 2d). In this time period, the intracellular cGAMP concentration remained constant, as did the cGAMP export activity (Extended Data Fig. 2e). Therefore, in this cell line, cGAMP is not exported by exocytosis or ATP-hydrolyzing pumps, but rather by an ATP-independent transporter or channel, likely driven by the electrochemical gradient

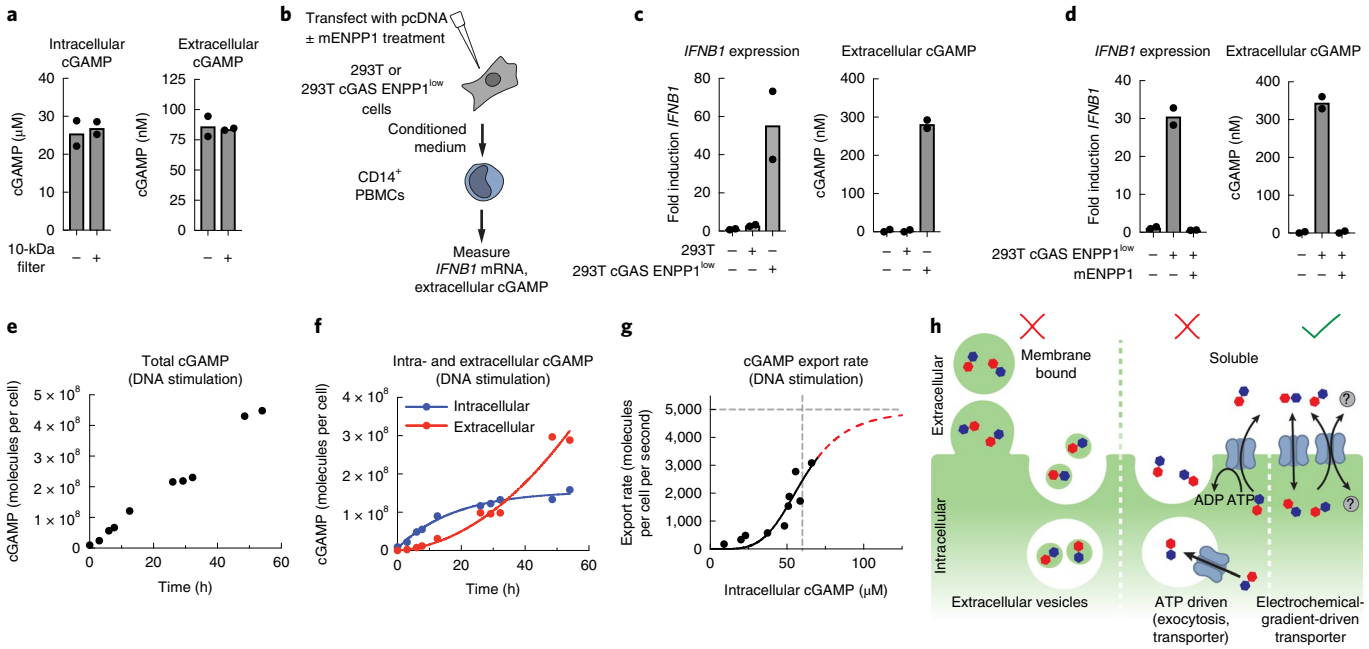

Fig. 2 | Characterization of cGAMP export mechanism in 293T cGAS *ENPP1*$^{-/-}$ cells. a, Intracellular and extracellular cGAMP for 293T cGAS *ENPP1*$^{-/-}$ cells measured with or without filtering the medium (10-kDa MWCO). Data are from one experiment, representative of two independent experiments (Supplementary Fig. 2a); two cell culture replicates are plotted. **b**, Schematic of the experiments in **c** and **d**. 293T or 293T cGAS ENPP1^{low} cells were transfected with empty pcDNA6 (0.5 μg ml^{-1}) and left untreated or treated with 20 nM recombinant mENPP1. Conditioned medium was incubated with CD14$^+$ PBMCs for 16 h. **c**,**d**, Extracellular cGAMP and *IFNB1* expression (mRNA levels were normalized to *CD14* and fold induction was calculated relative to untreated CD14$^+$ cells). Data shown in each panel are from one experiment; two cell culture replicates are plotted. Data in **c** are representative of three independent validations (Supplementary Fig. 2b,c). Data in **d** are supported by data in Figs. 3b,e,h,j and 4a. **e**,**f**, The amount of total cGAMP (**e**) and of intracellular (exponential fit) and extracellular (polynomial fit) cGAMP (**f**) over time produced by 293T cGAS *ENPP1*$^{-/-}$ cells after transfection with empty pcDNA6 (1.5 μg ml^{-1}). Data and fits are from one experiment, representative of three independent validations (Supplementary Fig. 2d,e). **g**, cGAMP export rate plotted against intracellular concentration of cGAMP, reanalyzed from data in **f**. Data are fit with an allosteric sigmoidal model: $v_{export} = V_{max}[substrate]^n/((K_{half})^n + [substrate]^n)$, where V_{max} is the maximal transporter velocity, n is the Hill slope and K_{half} is the substrate concentration at half V_{max}. If we constrain $V_{max} < 5{,}000$ molecules per cell per second, then $K_m > 60$ μM. Analysis is from the same experiment shown in **e** and **f**, representative of three independent validations (Supplementary Fig. 2d,e). **h**, Potential mechanisms of cGAMP export. In **a**,**c** and **d**, replicates are plotted individually with a bar representing the mean.

across the cell membrane. To further characterize the kinetics of the dominant exporter, we varied intracellular cGAMP concentrations through dsDNA stimulation. Because there was no cGAMP degradation in the *ENPP1*$^{-/-}$ cell line, the total amount of cGAMP synthesized was the sum of intracellular and extracellular cGAMP (Fig. 2e,f). The synthesis rate was linear for the first 12 h and then slowed slightly, possibly owing to loss of the dsDNA–cGAS complex over time. By plotting export rate as a function of intracellular cGAMP concentration, we observed that v_{export} did not plateau in the concentration range we tested (Fig. 2g). These kinetics are characteristic of a channel (no measurable K_m) or an allosterically controlled transporter with $V_{max} > 5{,}000$ molecules per cell per second and $K_m > 60$ μM, as the curve appeared sigmoidal instead of hyperbolic. This characterization will aid in future identification of cGAMP exporter(s) (Fig. 2h).

Development of a cell-impermeable ENPP1 inhibitor to enhance extracellular cGAMP activity. Having established the presence of extracellular cGAMP by carefully removing sources of ENPP1 from culture conditions, we determined whether intracellular and/or extracellular cGAMP is degraded by ENPP1. Despite its extracellular annotation, it is possible that ENPP1 could flip orientation on the membrane, as reported for a related enzyme, CD38 (ref. [29]), or that it could be active when being synthesized in the ER lumen and cGAMP might cross the ER membrane. To investigate the localization of ENPP1 activity, we transfected 293T cGAS *ENPP1*$^{-/-}$ cells with human *ENPP1* expression plasmid and confirmed its activity in whole-cell lysates (Fig. 3a). In intact cells, ENPP1 expression depleted extracellular cGAMP, but did not affect the intracellular cGAMP concentration (Fig. 3b). Therefore, only extracellular cGAMP is regulated by ENPP1 in these cells. However, we cannot exclude the possibility that ENPP1 has intracellular activity in other cell types or under certain stimulations (Fig. 3c).

To study the physiological relevance of extracellular cGAMP, we sought to develop cell-impermeable ENPP1 inhibitors that affect only extracellular ENPP1 activity. We first tested a nonspecific ENPP1 inhibitor, QS1 (refs. [30,31]; Extended Data Fig. 3a,b). QS1 can inhibit extracellular cGAMP degradation in cells overexpressing ENPP1. However, in ENPP1-null cells, QS1 also increased intracellular cGAMP and decreased extracellular cGAMP concentrations, suggesting that it blocks the cGAMP exporter(s) (Extended Data Fig. 3c). This export blockage activity excludes QS1 as a tool to study extracellular cGAMP. We therefore designed a phosphonate analog, STF-1084, to chelate Zn^{2+} at the ENPP1 catalytic site and to minimize cell permeability and avoid intracellular off-target effects (Fig. 3d). STF-1084 was 60-fold more potent than QS1 ($K_{i,app} = 110$ nM in an in vitro biochemical assay) (Fig. 3e and Extended Data Fig. 3b).

We confirmed that STF-1084 was cell impermeable by performing three independent permeability assays: the parallel artificial membrane permeability assay (PAMPA), the Caco-2 intestinal cell permeability assay and the MDCK epithelial cell permeability

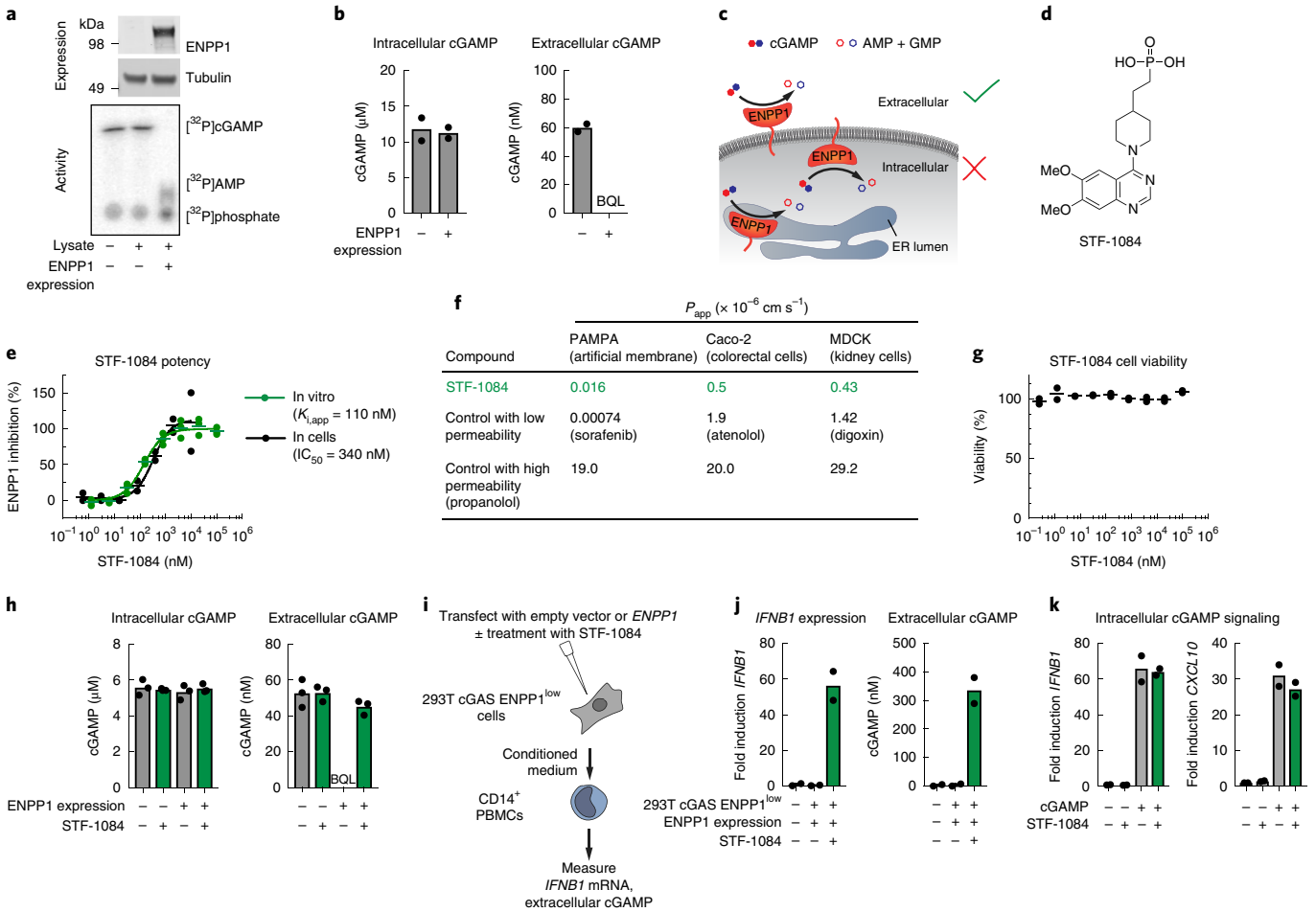

Fig. 3 | Development of a cell-impermeable ENPP1 inhibitor to enhance extracellular cGAMP activity. a,**b**, 293T cGAS *ENPP1*$^{-/-}$ cells were transfected with pcDNA6 (empty or encoding human *ENPP1*). ENPP1 expression and activity ([^{32}P]cGAMP hydrolysis by thin-layer chromatography (TLC), pH 9.0) (**a**; full scan of blot available as source data) and cGAMP concentrations (**b**) are shown. Data are from one experiment, representative of three independent validations (Supplementary Fig. 3a–d); two cell culture replicates are plotted in **b**. **c**, Possible cellular locations of ENPP1. **d**, Structure of the ENPP1 inhibitor STF-1084. **e**, Inhibition by STF-1084 in vitro ([^{32}P]cGAMP TLC assay, pH 7.5, purified mouse ENPP1: $K_{i,app}$ = 110 nM; three independent experiments are plotted) and in cells (cGAMP export assay, human ENPP1 transfected into 293T cGAS *ENPP1*$^{-/-}$ cells: IC_{50} = 340 nM; data are from one experiment; two cell culture replicates are plotted; supported by data in **h** and **j**). **f**, Mean apparent permeability (P_{app}) for STF-1084 and controls. For PAMPA and MDCK, the mean was calculated from two cell culture replicates in one experiment. For Caco-2, the mean was calculated from two independent experiments. **g**, PBMCs were incubated with STF-1084 for 16 h and viability was assessed. Data are from one experiment, representative of two independent validations (Supplementary Fig. 3e); three cell culture replicates are plotted. **h**, Intracellular and extracellular cGAMP for 293T cGAS *ENPP1*$^{-/-}$ cells transfected with pcDNA6 (empty or encoding human *ENPP1*) and left untreated or treated with 10 μM STF-1084 after 24 h. Data are from one experiment, representative of two independent validations (Supplementary Fig. 3f); three cell culture replicates are plotted. **i**, Schematic of the experiment in **j**. 293T cGAS ENPP1^{low} cells were transfected with human *ENPP1* and left untreated or treated with 10 μM STF-1084. Conditioned medium was incubated with CD14$^+$ PBMCs for 16 h. **j**, Extracellular cGAMP and *IFNB1* expression (mRNA levels were normalized to *CD14* and fold induction was calculated relative to untreated CD14$^+$ cells). Data are from one experiment (supported by data in **b**,**e**,**h** and Figs. 2d and 4a); two cell culture replicates are plotted. **k**, PBMCs were electroporated with control or with 200 nM cGAMP and incubated with or without 50 μM STF-1084 for 16 h. *IFNB1* and *CXCL10* mRNA levels were normalized to *ACTB* and fold induction was calculated relative to untreated cells. Data are from one experiment, representative of two independent experiments (Supplementary Fig. 3g,h); two cell culture replicates are plotted. In **b**,**e**,**g**,**h**,**j** and **k**, replicates are plotted individually with a bar representing the mean.

assay (Fig. 3f and Extended Data Fig. 3d). In comparison to control compounds with high or low cell permeability, STF-1084 fell into the category of impermeable compounds in all three assays. In addition, it had low activity toward the closely related ectonucleotidases alkaline phosphatase ($K_{i,app}$ > 100 μM) and ENPP2 ($K_{i,app}$ = 5.5 μM) (Extended Data Fig. 3e). Although we did not expect STF-1084 to have intracellular off-target effects owing to its low cell permeability, we tested its binding against a panel of 468 kinases to further determine its specificity. Despite its structural similarity to AMP, STF-1084 bound weakly to only two kinases at a 1 μM concentration (Extended Data Fig. 3f). STF-1084 also showed high stability (half-life of >159 min) in both human and mouse liver microsomes and was nontoxic to primary human PBMCs at a 100 μM concentration (Fig. 3g). Taking these findings together, we demonstrated that STF-1084 is a potent, cell-impermeable, specific, stable and nontoxic ENPP1 inhibitor.

Next, we measured the efficacy of STF-1084 in maintaining extracellular cGAMP concentrations of ENPP1-overexpressing 293T cGAS cells and obtained a half-maximal inhibitory concentration (IC_{50}) of 340 nM, with 10 μM being sufficient to completely block extracellular cGAMP degradation (Fig. 3e). Unlike QS1, STF-1084 had no effect on intracellular cGAMP, demonstrating

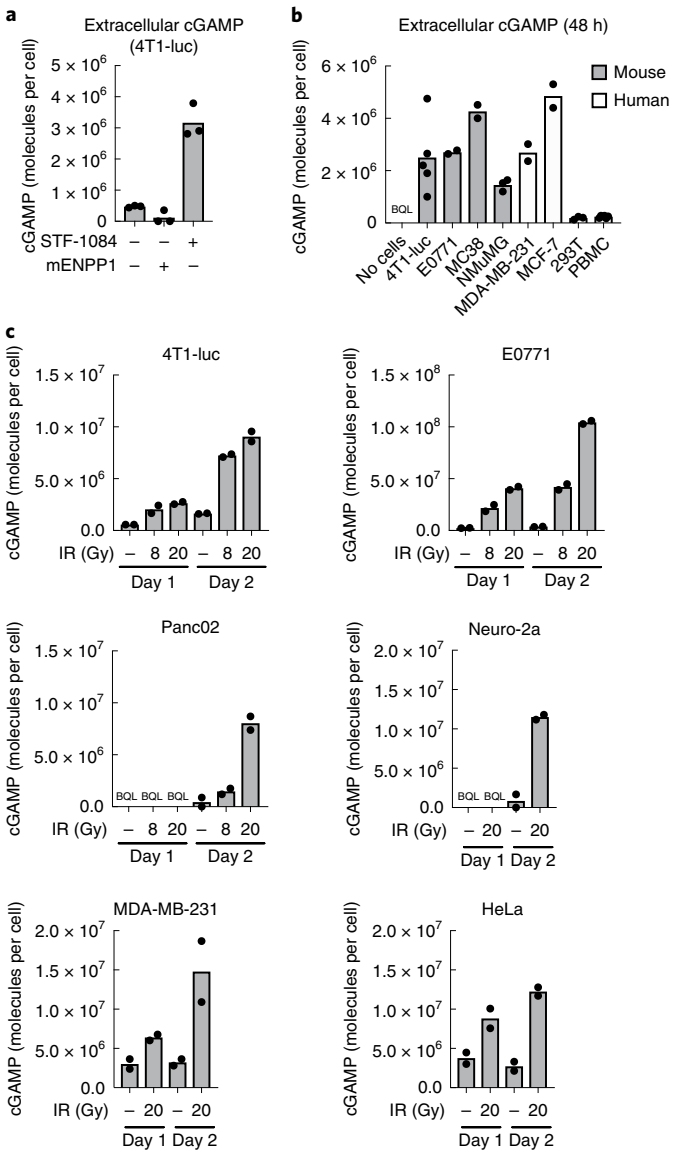

Fig. 4 | Cancer cells continuously export cGAMP in culture at steady state and ionizing radiation further increases export. a, Extracellular cGAMP produced by 4T1-luc cells after 48 h in serum-containing medium in the absence or presence of 50 μM STF-1084. Conditioned medium without STF-1084 was also incubated with 10 nM recombinant mENPP1 overnight. Data are from one experiment (supported by data in Fig. 3b,e,h,j); three cell culture replicates are plotted. **b**, Extracellular cGAMP produced by 4T1-luc (five cell culture replicates from two independent experiments), E0771 (two cell culture replicates), MC38 (two cell culture replicates), NMuMG (three cell culture replicates), MDA-MB-231 (two cell culture replicates), MCF-7 (two cell culture replicates), 293T (three cell culture replicates) and primary human PBMC (six cell culture replicates from two donors) cells measured after 48 h in the presence of 50 μM STF-1084. Data are from one experiment except where indicated for 4T1-luc cells. **c**, Extracellular cGAMP produced by the 4T1-luc, E0771, Panc02, Neuro-2a, MDA-MB-231 and HeLa cancer cell lines after 24 and 48 h. At time 0, cells were left untreated or were treated with IR (8 or 20 Gy) and refreshed with medium supplemented with 50 μM STF-1084. Data for each cell line are from one experiment. For 4T1-luc and E0771 cells, data are representative of two independent validations (Supplementary Fig. 4); two cell culture replicates are shown. In all panels, cGAMP was measured by LC–MS/MS and replicates are plotted individually with a bar representing the mean.

that it does not affect cGAMP export (Fig. 3h). Finally, we tested the efficacy of STF-1084 in boosting the extracellular cGAMP signal detectable to CD14$^+$ PBMCs. Conditioned medium from ENPP1-overexpressing 293T cGAS cells failed to induce *IFNB1* expression in CD14$^+$ cells (Fig. 3i,j). Presence of STF-1084 rescued extracellular cGAMP levels in the medium and induction of *IFNB1* expression in CD14$^+$ cells (Fig. 3j). STF-1084 had no effect on cytokine production when cGAMP was electroporated into primary human PBMCs (Fig. 3k), demonstrating that STF-1084 only boosts extracellular cGAMP signaling by preventing its degradation by ENPP1.

cGAMP export by cultured cancer cells is continuous at steady state and can be induced by ionizing radiation. Chromosomal instability of cancer cells has been reported to lead to micronucleus formation and rupture in the cytosol, and cGAS accumulates at these regions[25–27,32]. With STF-1084 as a specific extracellular ENPP1 inhibitor, we were poised to test whether cancer cells produce cGAMP and export it. In unstimulated 4T1-luc cells (a mouse triple-negative metastatic cancer cell line with a luciferase reporter), we were able to detect 350,000 molecules per cell (~150 nM) of intracellular cGAMP (Extended Data Fig. 4a). When we knocked down cGAS in these cells and reduced its protein level by approximately threefold, we also detected a reduction in cGAMP concentration of threefold (Extended Data Fig. 4a). In addition, we detected 350,000 molecules per cell of extracellular cGAMP in the medium after 48 h (Fig. 4a). Incubating the medium with recombinant mENPP1 abolished the cGAMP signal, demonstrating that extracellular cGAMP is in a free, soluble form (Fig. 4a). Strikingly, when we used STF-1084 to inhibit cell-surface and soluble ENPP1 in the cell culture medium, we measured 3,000,000 molecules per cell of extracellular cGAMP after 48 h (Fig. 4a). This is approximately tenfold more than the amount of intracellular cGAMP, demonstrating that these cells export at least 90% of the cGAMP they synthesize every 48 h. We detected similar levels of extracellular cGAMP in mouse (4T1-luc, E0771 and MC38) and human (MDA-MB-231 and MCF-7) cancer cell lines, as well as in immortalized normal mouse mammary gland (NMuMG) cells (Fig. 4b). In contrast, we detected much lower extracellular cGAMP levels in 293T cells, which have very low cGAS expression, and in primary human PBMCs, which have high cGAS expression but likely no cytosolic dsDNA to stimulate cGAS activity (Fig. 4b). We measured export over time in MC38 cells, and it followed linear kinetics as observed in our model 293T cGAS *ENPP1*$^{-/-}$ cells (Extended Data Fig. 4b). Besides 4T1-luc cells, the cells we tested (E0771, NMuMG and Panc02 cells) had intracellular cGAMP levels below our limit of detection, corresponding to less than ~40 nM intracellular cGAMP (Extended Data Fig. 4c). Interestingly, of the cell lines that we tested for intracellular cGAMP, only 4T1-luc cells had undetectable amounts of STING protein (Extended Data Fig. 4d). It is possible that cancer cells upregulate their cGAMP export mechanism(s) to clear intracellular cGAMP as a means to avoid activation of their own STING and subsequent IFN-β production.

IR, as a standard cancer treatment, has been shown to increase erroneous chromosomal segregation and cytosolic DNA[25–27,33,34]. Indeed, IR increased extracellular cGAMP production in all the cancer cell lines we tested (4T1-luc, E0771, Panc02, Neuro-2a, MDA-MB-231 and HeLa) (Fig. 4c) while causing negligible amounts of cell death (Extended Data Fig. 4e). Interestingly, IR induced more than tenfold higher extracellular cGAMP levels in E0771 cells than in the other cell lines, despite similar levels of basal extracellular cGAMP. Together, our data demonstrate that both mouse and human cancer cells, regardless of their tissue of origin, constantly produce and efficiently export cGAMP and can be stimulated with IR to produce more extracellular cGAMP.

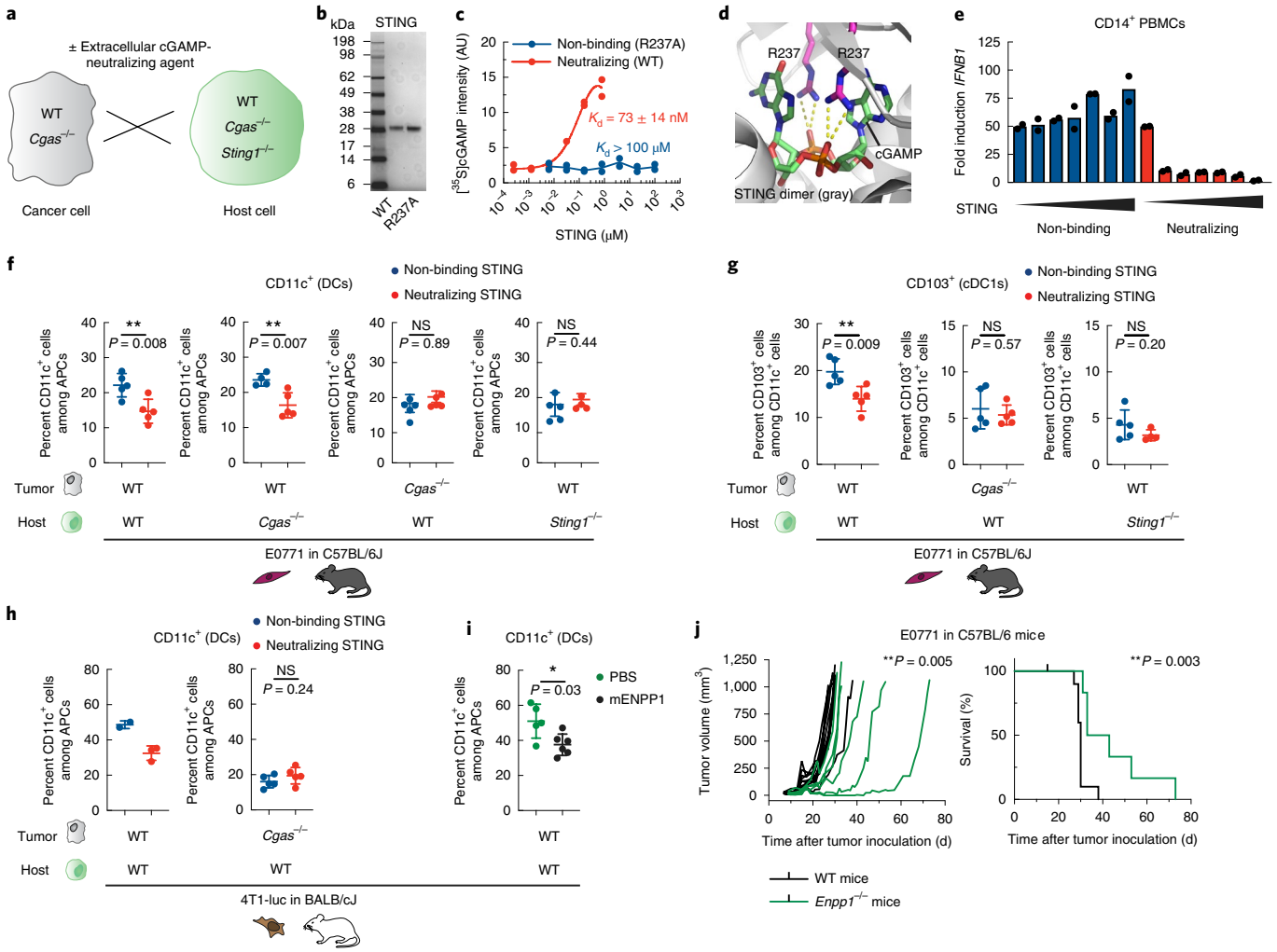

Fig. 5 | Extracellular cGAMP is produced by cancer cells and sensed by host STING. a, Experimental setup to assess the role of extracellular cGAMP in vivo. **b**, Coomassie gel of recombinant cytosolic mouse WT and R237A STING. Data are representative of five independent experiments. **c**, Binding curves for neutralizing STING (WT) and non-binding STING (R237A) determined by a membrane binding competition assay with [^{35}S]cGAMP. Data from two independent experiments are plotted. AU, arbitrary units. **d**, Structure of WT STING with cGAMP; the position of R237 is highlighted in pink (PDB 4LOJ). **e**, Fold induction of *IFNB1* mRNA in CD14$^+$ PBMCs treated with 2 μM cGAMP in the presence of neutralizing or non-binding STING (2–100 μM, 2.5-fold dilutions). Data are from one experiment (supported by data in Extended Data Fig. 5b–d); two qPCR replicates are plotted with a bar representing the mean. **f–i**, The indicated cells (1×10^6 for E0771 or 1×10^6 for 4T1-luc) of the indicated genetic background (WT or *Cgas*$^{-/-}$) were orthotopically injected into mice (C57BL/6 for E0771 and BALB/cJ for 4T1-luc) of the indicated genetic background (WT, *Cgas*$^{-/-}$ or *Sting1*$^{-/-}$) on day 0. Non-binding STING, neutralizing STING, PBS or recombinant mENPP1 was intratumorally injected on day 2. Tumors were collected and analyzed by flow cytometry on day 3. Sample sizes of *n* mice, from left to right (non-binding STING, neutralizing STING), were as follows: *n* = 5, 5; 4, 5; 5, 5; 5, 4 (**f**); *n* = 5, 5; 5, 5; 5, 4 (**g**); *n* = 2, 3; 5, 5 (**h**); *n* = 5, 6 (**i**). Data are shown as the mean ± s.d.; *P* values were determined by unpaired two-tailed *t* test with Welch's correction. **j**, E0771 cells (5×10^4) were orthotopically injected into WT (*n* = 10 mice) or *Enpp1*$^{-/-}$ (*n* = 6 mice) C57BL/6J mice. The *P* value for tumor volume was determined by pairwise comparisons using post hoc tests with a Tukey adjustment, while the *P* value for the Kaplan–Meier curve was determined by log-rank Mantel–Cox test.

Extracellular cGAMP produced by cancer cells and sensed by host STING is responsible for the curative effect of ionizing radiation. We next directly probed the physiological function of extracellular cGAMP in mouse models. First, to determine the importance of cancer versus host cGAMP, we knocked out *Cgas* in cancer cells (Extended Data Fig. 5a) and utilized *Cgas*$^{-/-}$ and *Sting1*$^{-/-}$ mice in the C57BL/6 background (Fig. 5a). We also developed a neutralizing protein agent, which should not be cell permeable, as a tool to specifically sequester extracellular cGAMP. We took advantage of the soluble cytosolic domain of STING (Fig. 5b), which binds cGAMP with a K_d of 73 ± 14 nM (Fig. 5c). We also generated R237A mutant STING[17] as a non-binding STING control (Fig. 5b–d). In cGAMP-treated human CD14$^+$ PBMCs, wild-type (WT) STING (neutralizing) was able to neutralize extracellular cGAMP with the predicted 2:1 stoichiometry, while the non-binding STING had no effect (Fig. 5e and Extended Data Fig. 5b). We observed similar results in primary mouse bone marrow cells (Extended Data Fig. 5c,d), validating in vitro the use of the STING proteins as tools to probe extracellular cGAMP.

We established E0771 orthotopic tumors in mice, followed by intratumoral injection of neutralizing STING to deplete extracellular cGAMP and excision of the tumors to stain for tumor-associated leukocytes. In WT E0771 tumors, neutralizing STING significantly decreased the CD11c$^+$ (dendritic cell, DC) and CD103$^+$CD11c$^+$ (conventional type 1 dendritic cell, cDC1) populations[35] among the CD45$^+$ major histocompatibility complex class II (MHC-II)$^+$ (tumor-associated antigen-presenting cell, APC) population (Fig. 5f,g and Extended Data Fig. 6a). This suggests that

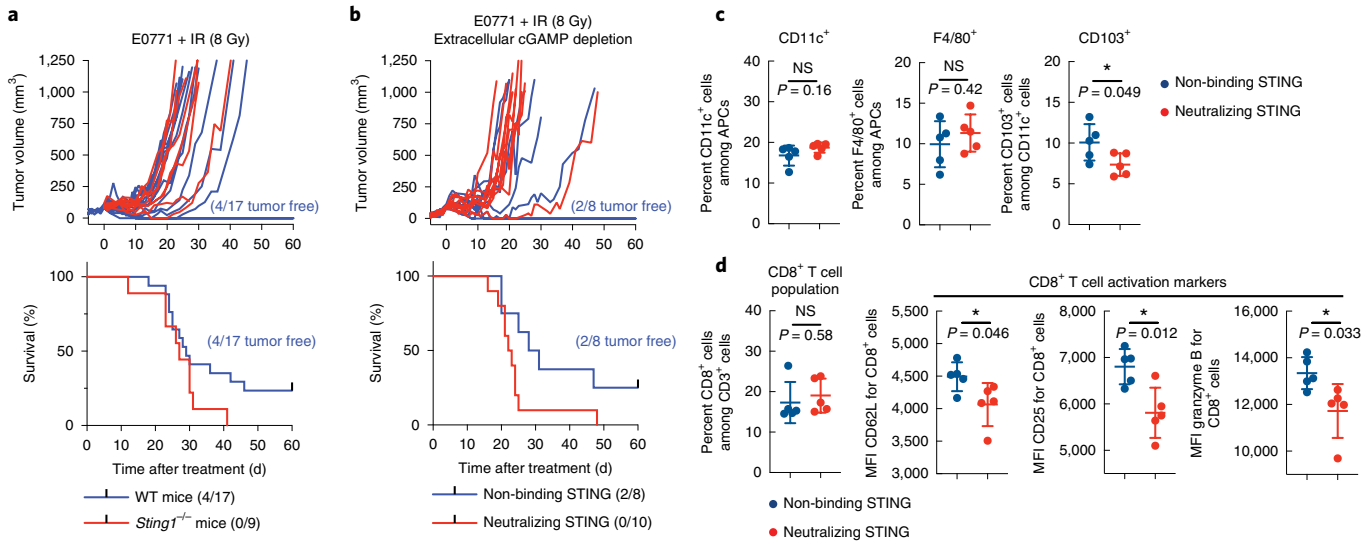

Fig. 6 | Extracellular cGAMP is responsible for the efficacy of ionizing radiation. a, E0771 cells (5×10^4) were orthotopically injected into WT ($n=17$ mice) or *Sting1*$^{-/-}$ ($n=9$ mice) C57BL/6J mice. Tumors were treated with IR (8 Gy) when they reached 100 ± 20 mm^3. Tumor volumes for individual mice and survival are plotted. **b**, E0771 cells (5×10^4) were orthotopically injected into WT C57BL/6J mice. Tumors were treated with IR (8 Gy) when they reached 100 ± 20 mm^3 and injected with non-binding ($n=8$ mice) or neutralizing ($n=10$ mice) STING every other day for the duration of the experiment. Tumor volumes for individual mice and survival are plotted. **c**,**d**, E0771 cells (5×10^4) were orthotopically injected into WT C57BL/6J mice. Tumors were treated with IR (8 Gy) when they reached 100 ± 20 mm^3 and injected with non-binding ($n=5$ mice) or neutralizing ($n=5$ mice) STING on days 2 and 4 after IR. Tumors were collected and analyzed by flow cytometry on day 5 to quantify populations of CD11c$^+$, F4/80$^+$, CD103$^+$ and CD8$^+$ cells, and activation markers of CD8$^+$ cells. Data are shown as the mean ± s.d.; *P* values were determined by unpaired two-tailed *t* test. MFI, mean fluorescence intensity.

extracellular cGAMP can be detected by the immune system to activate DCs that are important for the anticancer response[35]. Extracellular cGAMP depletion also diminished the CD11c$^+$ population when tumors were grown in *Cgas*$^{-/-}$ mice, suggesting that host cells do not contribute substantially to extracellular cGAMP production (Fig. 5f). In contrast, extracellular cGAMP depletion did not affect the CD11c$^+$ or CD103$^+$CD11c$^+$ population when *Cgas*$^{-/-}$ E0771 cells or *Sting1*$^{-/-}$ mice were used (Fig. 5f,g). Depleting extracellular cGAMP did not affect the proportion of the F4/80$^+$ (macrophage) population among the APC population in any of the experiments (Extended Data Fig. 6b). Together, our data demonstrate that cancer cells, and not host cells, are the dominant producers of extracellular cGAMP, which is then sensed by host STING and leads to infiltration of DCs, in particular cross-presenting cDC1s.

We also tested the orthotopic 4T1-luc tumor model. Although *Cgas*- and *Sting1*-knockout strains have not been established in the BALB/c background, we knocked out *Cgas* in 4T1-luc cells. Intratumoral injection of neutralizing STING into WT 4T1-luc tumors significantly decreased the tumor-associated CD11c$^+$ population among the CD45$^+$MHC-II$^+$ population (Fig. 5h). In contrast, extracellular cGAMP depletion had no effect in *Cgas*$^{-/-}$ 4T1-luc tumors (Fig. 5h). As an orthogonal approach, we depleted extracellular cGAMP by intratumoral injection of mENPP1 protein (Extended Data Fig. 2c) and again observed a diminished proportion of CD11c$^+$ cells in the CD45$^+$MHC-II$^+$ population (Fig. 5i). Together, our results demonstrate that extracellular cGAMP is produced by cancer cell cGAS and sensed by host STING, which leads to increased immune cell infiltration.

We next tested whether this basal level of extracellular cGAMP can also limit tumor growth. Long-term administration of neutralizing STING compared to the non-binding STING control did not alter the course of tumor progression in the E0771 model (Extended Data Fig. 6c), suggesting that endogenous ENPP1-mediated degradation was sufficient to abolish the anticancer effect of cancer-derived extracellular cGAMP. E0771 cells did not have particularly high ENPP1 activity (Extended Data Fig. 6d), but ENPP1 is also expressed on host cells and present in the serum as a soluble form[16,24,36]. We therefore implanted WT E0771 cells into *Enpp1*$^{-/-}$ mice and, indeed, observed slower tumor growth, suggesting that host ENPP1 promotes tumor growth in this model (Fig. 5j).

We next tested the physiological role of endogenous extracellular cGAMP when stimulated by IR, without ENPP1 inhibition. It was previously reported that IR exerts tumor-shrinkage effects in a host-STING-dependent manner[37] and activates cGAS-dependent IFN-β production in cancer cells[25,26,38]. Indeed, IR treatment induced cytokine production in both 4T1-luc and E0771 cells (Extended Data Fig. 7). Because E0771 cells exported high levels of cGAMP upon IR treatment (Fig. 4c), we investigated the role of extracellular cGAMP in the tumor-shrinkage effect of IR in the E0771 breast tumor model. We did not observe a significant increase in dead cells or cleaved caspases in either CD45$^-$ or CD45$^+$ cells in response to treatment with IR (8 Gy) at 24 h, suggesting that IR does not directly kill cancer or immune cells (Extended Data Fig. 8a). Treating established E0771 tumors with 8 Gy of IR resulted in tumor-free survival in 4 of 17 mice, demonstrating the efficacy of IR in this model (Fig. 6a). No tumor-free survival was observed in *Sting1*$^{-/-}$ mice, confirming that the curative effect of IR depends on host STING in this model, but probably not on cytokines produced by cancer cells (Fig. 6a). We sequestered extracellular cGAMP by injecting neutralizing STING for the duration of the experiment, with non-binding STING as a control. Remarkably, depletion of extracellular cGAMP completely abolished the curative effect of IR (Fig. 6b), suggesting that extracellular-cGAMP-induced host STING activation accounts for the curative effect of IR in this model.

To probe the cellular mechanism of extracellular cGAMP, we excised established tumors 5 d after treating them with IR followed by extracellular cGAMP depletion and analyzed immune cell populations (Extended Data Fig. 8b). The amounts of tumor-infiltrating CD11c$^+$ and F4/80$^+$ cells were not significantly altered when extracellular cGAMP was depleted with neutralizing STING as compared to the non-binding STING control (Fig. 6c). However, the CD103$^+$CD11c$^+$ subpopulation decreased in abundance,

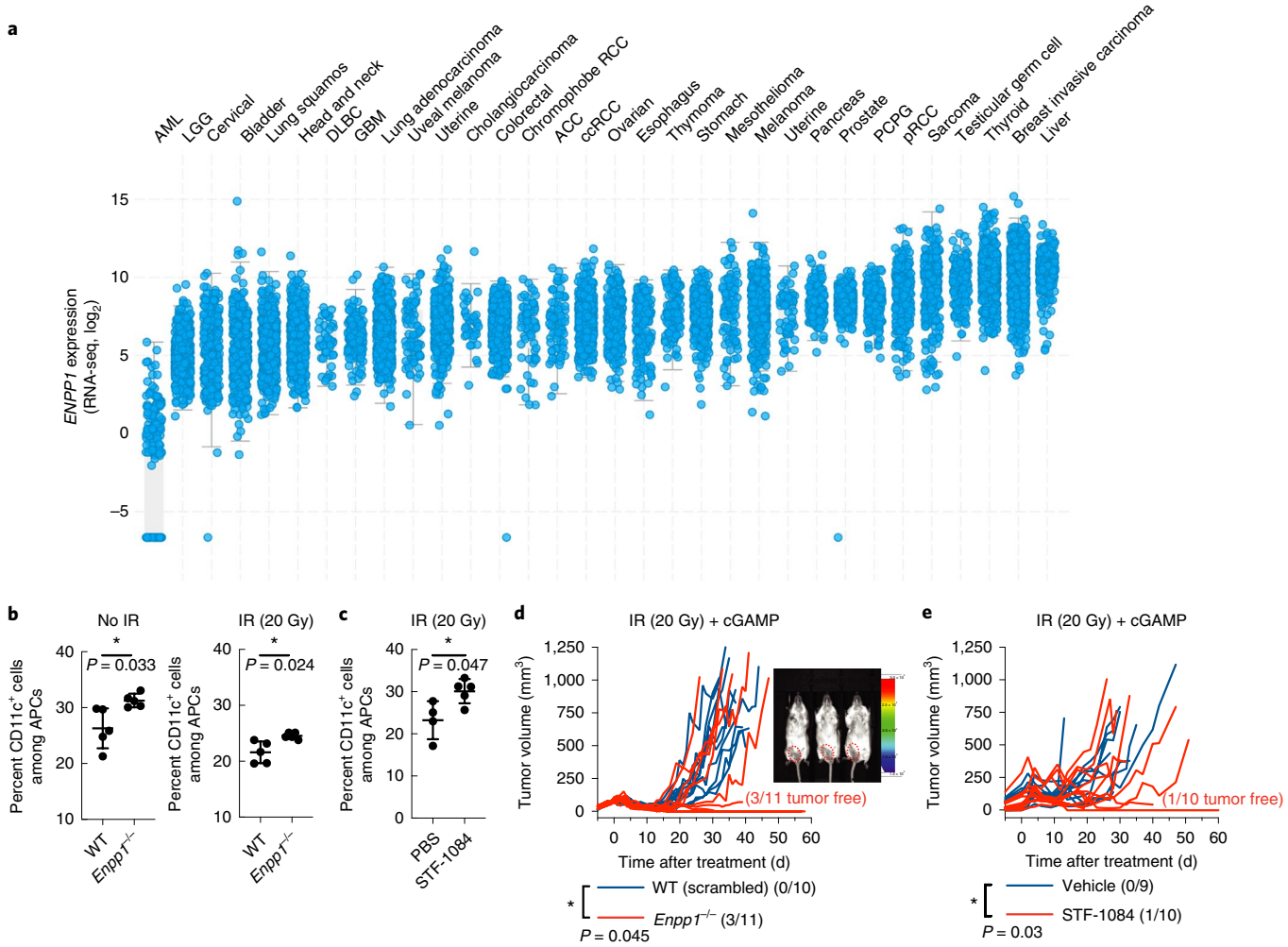

Fig. 7 | Genetic and pharmacological inhibition of ENPP1 increases immune detection of cancer and synergizes with ionizing radiation. a, *ENPP1* expression in human cancers. Data are represented as box plots showing ranges of mRNA expression levels. RNA sequencing data are from the TCGA Research Network (https://www.cancer.gov/tcga) PanCanAtlas and visualized with cBioPortal. **b**, WT or *Enpp1*$^{-/-}$ 4T1-luc cells (1×10^6) were orthotopically injected into WT BALB/cJ mice on day 0. Tumors were left untreated or treated with IR (20 Gy) on day 2. Tumors were collected and analyzed by flow cytometry on day 3. $n=5$ mice for all groups. Data are shown as the mean ± s.d.; *P* values were determined by unpaired two-tailed *t* test with Welch's correction. **c**, 4T1-luc cells (1×10^6) were orthotopically injected into WT BALB/cJ mice on day 0. Tumors were treated with IR (20 Gy) and intratumorally injected with PBS ($n=4$ mice) or STF-1084 ($n=5$ mice) on day 2. Tumors were collected and analyzed by flow cytometry on day 3. Data are shown as the mean ± s.d.; the *P* value was determined by unpaired two-tailed *t* test with Welch's correction. **d**, Established WT (harboring scrambled sgRNA) or *Enpp1*$^{-/-}$ 4T1-luc tumors (tumor volume of 100 ± 20 mm^3) were treated once with IR (20 Gy) followed by three intratumoral injections of 10 μg cGAMP on days 2, 4 and 7 after IR ($n=10$ mice for WT, $n=11$ mice for *Enpp1*$^{-/-}$). Tumor volumes for individual mice are shown; the *P* value was determined by pairwise comparisons using post hoc tests with a Tukey adjustment at day 20. In the *Enpp1*$^{-/-}$ 4T1-luc + IR (20 Gy) + cGAMP treatment group, 3 of 11 mice were tumor free, as verified by bioluminescence imaging (inset; tumor area outlined in red). **e**, Established 4T1-luc tumors (tumor volume of 100 ± 20 mm^3) were treated once with IR (20 Gy) followed by three intratumoral injections of 10 μg cGAMP alone ($n=9$ mice) or 10 μg cGAMP + 100 μl of 1 mM STF-1084 ($n=10$ mice) on days 2, 4 and 7 after IR. Tumor volumes for individual mice are shown; the *P* value was determined by pairwise comparisons using post hoc tests with a Tukey adjustment at day 40.

indicating weakened cross-presentation when extracellular cGAMP was depleted (Fig. 6c). Although the numbers of CD8$^+$ T cells were not altered significantly (Fig. 6d), expression levels of the activation markers CD62L, CD25 and granzyme B were dampened when extracellular cGAMP was depleted (Fig. 6d). Together, our results suggest that IR leads to complete tumor regression by increasing the extracellular cGAMP level, which then directly or indirectly increases the abundance of tumor-infiltrating cross-presenting cDC1s, leading to activation of CD8$^+$ cytotoxic T cells.

ENPP1 inhibitors synergize with IR to shrink tumors. ENPP1 is highly expressed in some breast cancers, and its level has been correlated with poor prognosis[39–41] (Fig. 7a). High ENPP1 expression may be a mechanism that breast cancers use to deplete extracellular cGAMP and dampen immune detection. We measured ENPP1 activity in three triple-negative breast cancer cell lines, 4T1-luc, E0771 and MDA-MB-231, of which MDA-MB-231 and 4T1-luc exhibited high ENPP1 activity (Extended Data Fig. 6d). We therefore chose the 4T1-luc mouse model to probe the effect of ENPP1 on tumor immune detection, growth and responses to treatment. We first tested the effect of ENPP1 on tumor-infiltrating DCs. Three days after implanting WT and *Enpp1*$^{-/-}$ tumors (Extended Data Fig. 9a) orthotopically in mice, we excised the tumors and analyzed their tumor-associated leukocyte composition.

Enpp1$^{-/-}$ tumors had a larger tumor-associated CD11c^{+} population than WT tumors when left untreated or treated with IR (20 Gy) (Fig. 7b). To further test that this effect was due to increased extracellular cGAMP, and not to potential membrane scaffolding effects of ENPP1, any unidentified intracellular activity or the 4T1-luc cells expressing Cas9 owing to the CRISPR knockout procedure, we used our cell-impermeable ENPP1 inhibitor. We intratumorally injected STF-1084 immediately after IR treatment and tested its effect after 24 h. Indeed, in comparison to vehicle control, STF-1084 mirrored the effect of *Enpp1* knockout by increasing the abundance of the tumor-associated CD11c^{+} population (Fig. 7c).

We then tested the effect of ENPP1 expressed by 4T1-luc cells on tumor rejection. We did not observe significant growth delay for 4T1-luc *Enpp1*$^{-/-}$ tumors as compared to WT tumors harboring a scrambled sgRNA when they were left untreated or treated with IR or intratumoral cGAMP injections individually (Extended Data Fig. 9b–d). Strikingly, 3 of 11 mice inoculated with *Enpp1*$^{-/-}$ tumors achieved tumor-free survival when treated with a combination of IR and cGAMP injections, whereas no mice inoculated with WT tumors survived (Fig. 7d). This demonstrates that ENPP1 expressed on the surface of 4T1-luc cells was sufficient to abolish the tumor-shrinkage effect of combination therapy. Taking these findings together, we have demonstrated that ENPP1 expressed on both cancer cells (4T1 model) and the host (E0771 model) has a role in clearing extracellular cGAMP and promotes tumor growth.

Although it is still an open question whether cancer or host ENPP1 has a bigger role, small-molecule inhibitors should, in principle, inhibit both. We tested the ENPP1 inhibitor STF-1084 in this combination therapy. STF-1084 has fast pharmacokinetics. Without optimizing its route of administration and pharmacokinetic properties, we intratumorally injected it into established orthotopic 4T1-luc tumors. STF-1084 synergized with IR and cGAMP to significantly delay tumor progression and resulted in tumor-free survival in one of ten mice (Fig. 7e).

Other than breast cancers, pancreatic cancers also express high levels of ENPP1 (Fig. 7a)[42,43]. To access these tumors, which are not easily accessible through intratumoral injections, we sought to develop an analog of STF-1084 that can be administered systemically. We developed STF-1623 (Extended Data Fig. 10a), with improved $K_{i,app}$ of 16 nM (Extended Data Fig. 10b). We performed a similar suite of assays on STF-1623 as we did on STF-1084. We confirmed that it is also cell impermeable (Extended Data Fig. 10c,d), is not toxic to primary human PBMCs (Extended Data Fig. 10e), does not target kinases (Extended Data Fig. 10f) and is stable to human and mouse microsomes (half-life of >159 min). In addition, STF-1623 affected only extracellular cGAMP concentrations (Extended Data Fig. 10g) and had no effect on cytokine production when cGAMP was electroporated into primary human PBMCs (Extended Data Fig. 10h). Notably, STF-1623 showed an improved pharmacokinetic profile when compared to STF-1084 for systemic dosing. With subcutaneous injections, we could achieve >100 nM plasma concentrations after 24 h (Extended Data Fig. 10i).

We then tested STF-1623 in the Panc02 syngeneic subcutaneous pancreatic tumor model. STF-1623 delayed tumor growth as a single agent and synergized with IR to delay tumor growth as well as achieve stable disease and tumor regression in some mice (Extended Data Fig. 10j). Because this Panc02 model is not metastatic, we predict that tumor regression would lead to increased survival. Future studies are needed to determine whether treatment with STF-1623 leads to a survival advantage in metastatic models. Together, our results demonstrate that the antitumor effect of extracellular cGAMP can be enhanced by inhibiting its degradation enzyme ENPP1. STF-1623 serves as a starting point for new classes of anticancer agents that can synergize with the endogenous extracellular cGAMP exported by cancer cells and induced by IR.

Discussion

Here we provide in vitro and in vivo evidence that cGAMP can signal through the extracellular space. In all the cell types we have tested, cGAMP can be exported at various levels, suggesting that cGAMP export is not a cancer-specific phenomenon and that cGAMP exporters are likely expressed in most cell types. Because chromosomal instability and aberrant cytosolic dsDNA are cancer-intrinsic properties[44,45] and cancer cells rarely inactivate cGAS[27], we reason that cGAMP overproduction and increased export may also be properties intrinsic to cancer cells. As no cytosolic cGAMP hydrolase has been identified and ENPP1 cannot degrade intracellular cGAMP, export is currently the only known mechanism by which cGAMP is removed from the cytosol and represents another way to turn off intracellular STING signaling in addition to ubiquitin-mediated STING degradation[46]. This clearance mechanism, however, exposes cancer cells to immune detection.

Indeed, our results demonstrate that cGAMP exported by cancer cells is a danger signal detected by the immune system. It is well known that neoantigens from cancer cells are presented by APCs to cross-prime the cytotoxic CD8^{+} T cells that eventually perform cancer-specific killing[7,18]. However, it is less understood how APCs initially detect cancer cells. It has been shown that immunogenic tumors release dsDNA as a danger signal to CD11c^{+} DCs[7,47]. The evidence for IFN as a danger signal is mixed: one study showed that cancer cells respond to their own cytosolic dsDNA induced by IR and produce IFNs as a danger signal[48], whereas other studies have reported that cancer cells can lose their ability to make IFN via the STING pathway or even repurpose the STING pathway to aid in metastasis[27,49]. A recent study showed that the catalytic activity of cancer cGAS correlated with anticancer immunity in the B16 melanoma model in a host-STING-dependent manner[15], but the mechanism of this suggested transfer of cGAMP from cancer to host cells was unknown. Here we provide direct evidence that cancer cells produce soluble extracellular cGAMP as a danger signal, which leads to increased numbers of DCs, specifically cross-presenting cDC1s, and cytotoxic T cell activation in the tumor microenvironment. cGAMP export is an important mode of cGAMP communication among cells that are not physically connected but are in close proximity. Unlike cytokines, it is unlikely that extracellular cGAMP can travel long distances in the extracellular space without being degraded and/or diluted to below its effective concentrations. We call cGAMP an immunotransmitter, owing to these shared properties with neurotransmitters and its immune signaling functions. Extracellular cGAMP should be studied both for its basic biology as an immunotransmitter and for its therapeutic potential in cancer.

Methods

Reagents and antibodies. [α-^{32}P]ATP (800 Ci mmol^{-1}, 10 mCi ml^{-1}, 250 µCi) and [^{35}S]ATPαS (1,250 Ci mmol^{-1}, 12.5 mCi ml^{-1}, 250 µCi) were purchased from PerkinElmer. ATP, GTP, [$^{13}C_{10}$,$^{15}N_5$]ATP, 4-nitrophenyl phosphate and bis(4-nitrophenyl) phosphate were purchased from Sigma-Aldrich. cGAMP and isotope-labeled cGAMP were synthesized as described previously[19]. The Caco-2 assay was purchased from Cyprotex. Kinome screens were conducted by Eurofins (data visualized with the TREEspot Software Tool). PAMPA and MDCK permeability assays were conducted by Quintara Discovery. Total protein content was quantified with the BCA assay (Thermo Fisher). Cell viability was quantified with the CellTiter-Glo assay (Promega) or the LDH assay (Pierce, Thermo Fisher). Mouse CXCL10 production was quantified by mouse CXCL10/IP-10/CRG-2 DuoSet ELISA (R&D Systems) and the TMB Substrate Reagent Set (BD Bioscience). Full-length human *ENPP1* was cloned into the pcDNA6 vector. QS1 was synthesized as previously described[31]. The following monoclonal antibodies were used for western blotting: rabbit anti-cGAS (D1D3G, Cell Signaling; 1:1,000 dilution), rabbit anti-mouse cGAS (D2O8O, Cell Signaling; 1:1,000 dilution), mouse anti-tubulin (DM1A, Cell Signaling; 1:2,000 dilution), rabbit anti-STING (D2P2F, Cell Signaling; 1:1,000 dilution), rabbit anti-phospho-IRF3 (4D4G, Cell Signaling; 1:1,000 dilution), rabbit anti-IRF3 (D83B9, Cell Signaling; 1:1,000 dilution), IRDye

800CW goat anti-rabbit (LI-COR; 1:15,000 dilution) and IRDye 680RD goat anti-mouse (LI-COR; 1:15,000 dilution).

Mammalian cell lines and primary cells. 293T, NMuMG, MDA-MB-231, HeLa, MCF-7 and Neuro-2a cells were procured from ATCC, Panc02 cells were procured from the DTP/DCTD/NCI Tumor Repository, E0771 cells were procured from CH3 BioSystems, 4T1-luciferase (4T1-luc) cells were a gift from C. Contag, Stanford University, Stanford, CA, USA[50] and HEK293S GnT1$^-$ cells expressing secreted mENPP1 were a gift from O. Nureki, University of Tokyo, Tokyo, Japan[51]. All cell lines were maintained in a 5% CO_2 incubator at 37 °C. 293T, Neuro-2a, MC38, MDA-MB-231, HeLa and L929 cells were maintained in DMEM (Corning Cellgro) supplemented with 10% FBS (Atlanta Biologics) and 100 U ml^{-1} penicillin-streptomycin (Thermo Fisher). NMuMG and MCF-7 cells were maintained in DMEM supplemented with 10% FBS, 100 U ml^{-1} penicillin-streptomycin and 10 µg ml^{-1} bovine insulin (MilliporeSigma). 4T1-luc and Panc02 cells were maintained in RPMI (Corning Cellgro) supplemented with 10% FBS and 100 U ml^{-1} penicillin-streptomycin. E0771 cells were maintained in RPMI supplemented with 10% FBS, 100 U ml^{-1} penicillin-streptomycin and 10 mM HEPES. Primary human PBMCs were isolated by subjecting enriched buffy coat from whole blood (Stanford Blood Center) to a Percoll density gradient. CD14$^+$ PBMCs were isolated with CD14$^+$ MicroBeads (Miltenyi). PBMCs were cultured in RPMI supplemented with 2% human serum and 100 U ml^{-1} penicillin-streptomycin. Primary mouse bone marrow cells were isolated by opening the ends of the femur and tibia and removing cells by centrifugation[52] and were cultured in RPMI supplemented with 10% FBS and 100 U ml^{-1} penicillin-streptomycin. Bone marrow cells were differentiated into bone marrow-derived macrophages by culturing as above plus 10% conditioned medium from L929 cells.

Cell line generation. 293T cells were virally transfected to stably express mouse or human cGAS. 293T cGAS ENPP1^{low} cells were created by viral transfection of CRISPR sgRNA targeting human *ENPP1* (5′-CACCGCTGGTTCTATGCACG TCTCC-3′), and 293T cGAS *ENPP1*$^{-/-}$ cells were selected after single-cell cloning from this pool. 4T1 and E0771 *Cgas*$^{-/-}$ cells were created by viral transfection of CRISPR sgRNA (using lentiCRISPRv2-blast, Addgene plasmid 83480; ref. [53]) targeting mouse *Cgas* (5′-CACCGGAAGGGGCGCGCGCTCCACC-3′). Cells were single-cell cloned, and multiple knockouts were pooled after verification by western blotting. 4T1-luc *Enpp1*$^{-/-}$ cells and cells with scrambled sgRNA were created by viral transfection of CRISPR sgRNAs (using lentiCRISPRv2-blast) targeting mouse *Enpp1* (5′-GCTCGCGCCCATGGACCT-3′ and 5′-ATATGACTGTACCCTACGGG-3′) or a scrambled sequence. Cells were selected with 0.5–2 µg ml^{-1} blasticidin and single-cell cloned, and multiple knockouts were pooled after verification by activity assay. Alternatively, 4T1-luc *Enpp1*$^{-/-}$ cells and cells with scrambled sgRNA were created by transient transfection with Lipofectamine 3000 of the same CRISPR sgRNAs as above or a scrambled sequence (using PX458, Addgene plasmid 48138), followed by single-cell cloning of GFP-positive cells. Multiple clean knockouts were pooled after verification by activity assay (commercial antibodies are not sensitive enough for verification of protein expression). 4T1-luc shcGAS cells were created by viral transfection of shRNA (5′-CAGGATTGAGCTACAAGAATAT-3′)[48] using plasmid pGH188. Cells harboring the shRNA were selected with 0.5–2 µg ml^{-1} blasticidin, sorted for GFP expression and used as a pool.

Expression and purification of recombinant proteins. sscGAS was produced as described previously[19]. mENPP1 was produced as described previously[51,54].

The coding sequence for mouse STING (residues 139–378) was inserted into the pTB146 His-SUMO vector (a generous gift from T. Bernhard, Harvard Medical School) and expressed in Rosetta cells. Cells were grown in 2× YT medium with 100 µg ml^{-1} ampicillin and induced when the OD_{600} reached 1 with 0.75 mM IPTG at 16 °C overnight. All subsequent procedures using proteins and cell lysates were performed at 4 °C. Cells were pelleted and lysed in 50 mM Tris pH 7.5, 400 mM NaCl, 10 mM imidazole, 2 mM DTT and protease inhibitors (cOmplete, EDTA-free protease inhibitor cocktail, Roche). Cells were lysed by sonication, and the lysate was cleared by ultracentrifugation at 50,000 RCF for 1 h. The cleared supernatant was incubated with HisPur cobalt resin (Thermo Fisher Scientific; 1 ml of resin per 1 liter of bacterial culture) for 30 min. The resin-bound protein was washed with 50 column volumes of 50 mM Tris pH 7.5, 150 mM NaCl and 2% Triton X-114, 50 column volumes of 50 mM Tris pH 7.5 and 1 M NaCl (each wash was set to a drip rate of 1 drop every 2–3 s and took 2–3 h) and 20 column volumes of 50 mM Tris pH 7.5 and 150 mM NaCl. Protein was eluted from the resin with 600 mM imidazole in 50 mM Tris pH 7.5 and 150 mM NaCl. Fractions containing His-SUMO–STING were pooled, concentrated and dialyzed against 50 mM Tris pH 7.5 and 150 mM NaCl while incubating with the SUMOlase enzyme His–ULP1 to remove the His-SUMO tag overnight. The solution was incubated with HisPur cobalt resin again to remove the His-SUMO tag, and STING was collected from the flow-through. Protein was dialyzed against 20 mM Tris pH 7.5, loaded onto a HitrapQ anion exchange column (GE Healthcare) with an Äkta FPLC (GE Healthcare) and eluted with a NaCl gradient. Fractions containing STING were pooled, and buffer was exchanged into PBS.

Liquid chromatography and tandem mass spectrometry. For measurement of cGAMP, cyclic GMP-[$^{13}C_{10}$,$^{15}N_5$]AMP was used as an internal standard at 0.5–1 µM. Samples were analyzed for cGAMP, ATP and GTP content on a Shimadzu HPLC with an autosampler set at 4 °C and connected to an AB Sciex 4000 QTRAP. A volume of 10 µl was injected onto a Biobasic AX LC column (5 µm, 50 × 3 mm; Thermo Scientific). The mobile phase consisted of 100 mM ammonium carbonate (A) and 0.1% formic acid in acetonitrile (B). The initial condition was 90% B, maintained for 0.5 min. The mobile phase was ramped to 30% A from 0.5 min to 2.0 min, maintained at 30% A from 2.0 min to 3.5 min, ramped to 90% B from 3.5 min to 3.6 min and maintained at 90% B from 3.6 min to 5 min. The flow rate was set to 0.6 ml min^{-1}. The mass spectrometer was operated in electrospray positive-ion mode with the source temperature set at 500 °C. Declustering and collision-induced dissociation were achieved with nitrogen gas. For each molecule, the MRM transition(s) (*m*/*z*), DP (V) and CE (V) were as follows: ATP (508 > 136, 341, 55), GTP (524 > 152, 236, 43), cGAMP (675 > 136, 121, 97; 675 > 312, 121, 59; 675 > 152, 121, 73), internal standard cyclic GMP-[$^{13}C_{10}$,$^{15}N_5$]AMP (690 > 146, 111, 101; 690 > 152, 111, 45; 690 > 327, 111, 47).

For STF-1084 and STF-1623, measurements were performed with a Q-Exactive FT mass spectrometer (Thermo) equipped with a Vanquish uHPLC. Samples were diluted in water with 0.1% formic acid and injected onto a Phenomenex Synergi Hydro-RP column (particle size of 4 µm, ID of 2 mm, length of 30 mm). The column compartment was at ambient temperature. The flow rate was 0.5 ml min^{-1}. Mobile phase A was water with 0.1% formic acid; mobile phase B was acetonitrile with 0.1% formic acid. Each run was 5 min; the gradient was as follows: 0–0.5 min, 0% B; 0.5–2 min, linear from 0% to 95% B; 2–3.5 min, hold at 95% B; 3.5–3.6 min, 95% B to 0% B; 3.6–5 min, 0% B to re-equilibrate the column. Data for minutes 1–4.8 were sent to the mass spectrometer for analysis. Detection on the Q-Exactive was performed in positive-ion mode between 100–1,000 *m*/*z*, using an acquisition target of 1 × 10^6 with maximum IT of 100 ms at a resolution of 70,000. Quantification was performed with TraceFinder 4.1 software (Thermo Fisher).

Export assays in 293T cGAS *ENPP1*$^{-/-}$ cells. 293T cGAS *ENPP1*$^{-/-}$ cells were plated on plates coated with PurCol (Advanced BioMatrix). In some experiments, cells were transfected with the indicated plasmids complexed with FuGENE 6 (Promega) 24 h before the export experiment. At the start of the experiment, the medium was replaced with serum-free DMEM supplemented with 1% insulin-transferrin-selenium-sodium pyruvate (Thermo Fisher) and 100 U ml^{-1} penicillin-streptomycin. At the indicated times, the medium and cells were removed and centrifuged at 1,000 RCF for 10 min at 4 °C. Cells were lysed in 30 to 100 µl of 50:50 acetonitrile:water supplemented with 500 nM internal standard and centrifuged at 15,000 RCF for 20 min at 4 °C. The medium was supplemented with internal standard at 500 nM and 20% formic acid. If medium cGAMP enrichment was necessary, the medium was acidified with 0.5% acetic acid, supplemented with internal standard and applied to HyperSep Aminopropyl SPE columns (Thermo Fisher Scientific) as described previously[22]. Eluents were evaporated to dryness and reconstituted in 50:50 acetonitrile:water. The medium and cell extract were submitted for mass spectrometry quantification of cGAMP, ATP and GTP.

Conditioned medium transfer. 293T cGAS ENPP1^{low} cells were plated and transfected with plasmid DNA as described above. Twenty-four hours after transfection, the medium was changed to RPMI supplemented with 2% human serum and 1% penicillin-streptomycin, with or without 2 µM cGAMP, 20 nM recombinant mENPP1 or 50 µM STF-1084. Twenty-four hours after the medium change, the conditioned medium was removed from 293T cGAS ENPP1^{low} cells and incubated with freshly isolated CD14$^+$ PBMCs. Gene expression of CD14$^+$ PBMCs was analyzed 14–16 h later.

PBMC electroporation of cGAMP and treatment with ENPP1 inhibitor. PBMCs (2 × 10^6) were resuspended in electroporation buffer (90 mM Na_2HPO_4, 90 mM NaH_2PO_4, 5 mM KCl, 10 mM $MgCl_2$ and 10 mM sodium succinate) with or without 200 nM cGAMP. Cells were electroporated in a cuvette with a 0.2-cm electrode gap (Bio-Rad) by using program U-013 on a Nucleofector II device (Lonza) and immediately transferred to fresh medium with or without ENPP1 inhibitor.

RT–PCR analysis. Total RNA was extracted with TRIzol (Thermo Fisher Scientific) and reverse transcribed with Maxima H Minus Reverse Transcriptase (Thermo Fisher Scientific). Real-time PCR was performed in duplicate with AccuPower 2× Greenstar qPCR Master Mix (Bioneer) on a 7900HT Fast Real-Time PCR System (Applied Biosystems). Data were normalized to *CD14*, *ACTB* or *GAPDH* expression (human) and *Actb* expression (mouse) for each sample. Fold induction was calculated by $\Delta\Delta C_t$. Primers used were as follows: human *IFNB1*: forward, 5′-AAACTCATGAGCAGTCTGCA-3′; reverse, 5′-AGGAGAT CTTCAGTTTCGGAGG-3′; human *CXCL10* (ref. [9]): forward, 5′-TCTGAATCC AGAATCGAAGG-3′; reverse, 5′-CTCTGTGTGGTCCATCCTTG-3′; human *CD14*: forward, 5′-GCCTTCCGTGTCCCCACTGC-3′; reverse, 5′-TGAGGGGG CCCTCGACG-3′; human *ACTB*: forward, 5′-GGCATCCTCACCCTGAAGTA-3′; reverse, 5′-AGAGGCGTACAGGGATAGCA-3′; human *GAPDH*: forward, 5′-CC AAGGTCATCCATGACAAC-3′; reverse, 5′-CAGTGAGCTTCCCGTTCAG-3'; mouse *Cxcl10* (ref. [9]): forward, 5′-CTCTGTGTGGTCCATCCTTG-3′; reverse,

5′-GTGGCAATGATCTCAACACG-3′; mouse *Actb*[9]: forward, 5′-AGCCATGT ACGTAGCCATCC-3′; reverse, 5′-CTCTCAGCTGTGGTGGTGAA-3′.

[^{32}P]cGAMP degradation thin-layer chromatography assays. Radiolabeled [^{32}P] cGAMP was synthesized as previously described[16]. Cell lysates were generated by scraping and lysing 1×10^6 cells (293T) or 10×10^6 cells (4T1-luc, E0771 and MDA-MB-231) in 100 µl of 10 mM Tris, 150 mM NaCl, 1.5 mM $MgCl_2$ and 1% NP-40, pH 9.0. Samples were normalized to the amount of protein in each lysate reaction. Probe ([^{32}P]cGAMP; 5 µM) was incubated with mENPP1 (20 nM) or whole-cell lysate in 100 mM Tris, 150 mM NaCl, 2 mM $CaCl_2$ and 200 µM $ZnCl_2$, pH 7.5 or 9.0, for the indicated amount of time. To generate inhibition curves, fivefold dilutions of ENPP1 inhibitor were included in the reaction. Degradation was evaluated by TLC as previously described[16]. Plates were exposed on a phosphor screen (Molecular Dynamics) and imaged on a Typhoon 9400, and the ^{32}P signal was quantified with ImageJ. Inhibition curves were fit to obtain IC_{50} values with GraphPad Prism 7.03. IC_{50} values were converted to $K_{i,app}$ values by using the Cheng–Prusoff equation: $K_{i,app} = IC_{50}/(1 + [substrate]/K_m)$.

ALPL and ENPP2 inhibition assays. Inhibition assays were performed by monitoring production of 4-nitrophenolate by absorbance at 400 nm. ALPL conditions: 0.1 nM ALPL, 2 µM 4-nitrophenyl phosphate and inhibitor in buffer (pH 9.0) containing 50 mM Tris, 20 µM $ZnCl_2$ and 1 mM $MgCl_2$ at room temperature. ENPP2 conditions: 2 nM ENPP2, 500 µM bis(4-nitrophenyl) phosphate and inhibitor in buffer (pH 9.0) containing 100 mM Tris, 150 mM NaCl, 200 µM $ZnCl_2$ and 2 mM $CaCl_2$.

Intracellular and extracellular cGAMP measurement in cancer cell lines. Cells were refreshed at time 0 with medium supplemented with 50 µM STF-1084 (for IR experiments, cancer cell lines were also exposed to 8 or 20 Gy of gamma radiation from a cesium source). At the indicated times, medium and cells were collected and centrifuged at 1,000 RCF. Cells were counted, lysed with solution containing 78% water, 20% methanol and 2% acetic acid and centrifuged at 15,000 RCF. cGAMP was enriched from the medium and cell extract as described above.

Mouse models (4T1-luc, E0771 and Panc02). Five- to 9-week-old female mice were used for all experiments, and all tumor inoculations were performed with PBS as the vehicle. BALB/c mice (Jackson Laboratories) were inoculated with 5×10^4 or 5×10^5 4T1-luc or 4T1-luc *Enpp1*$^{-/-}$ cells suspended in 50 µl in the fifth mammary fat pad. WT, *Sting1*$^{gt/gt}$ (referred to as *Sting1*$^{-/-}$) and *Enpp1*$^{-/-}$ C57BL6/J mice (Jackson Laboratories) were inoculated with 5×10^4 E0771 cells suspended in 50 µl in the fifth mammary fat pad. C57BL6/J mice were inoculated with 3×10^6 Panc02 cells suspended in 100 µl subcutaneously in the right hind flank. When tumor volume (determined by length^2 × width/2) reached 100 ± 20 mm^3, tumors were irradiated with 20 Gy (4T1-luc and Panc02) or 8 Gy (E0771) from a 225-kVp cabinet X-ray irradiator filtered with 0.5-mm Cu (IC-250, Kimtron). Anesthetized animals were shielded with a 3.2-mm lead shield with a 15×20 mm^2 aperture where the tumor was placed. For Panc02, the mice were implanted subcutaneously between the scapulae with an osmotic pump (Alzet, 1002) containing a solution of 200 mg ml^{-1} STF-1623 in PBS or PBS alone 1 d before IR. Pumps were removed 8 d after implantation. Treatments after irradiation were administered as specified. Tumor volumes were recorded and analyzed in a generalized estimation equation to account for within-mouse correlation. Pairwise comparisons of the treatment groups at each time point were done by using post hoc tests with a Tukey adjustment for multiple comparisons. Animal death was plotted in a Kaplan–Meier curve with GraphPad Prism 7.03, and statistical significance was assessed by log-rank Mantel–Cox test. Mice were maintained at Stanford University in compliance with Stanford University Institutional Animal Care and Use Committee regulations and procedures were approved by the Stanford University administrate panel on laboratory animal care, or mice were maintained by Crown Biosciences in accordance with their regulations on animal laboratory care.

Flow cytometry analysis of tumors. WT BALB/c (4T1-luc tumors) and WT, *Cgas*$^{-/-}$ or *Sting1*$^{-/-}$ C57BL/6 (E0771 tumors) mice were inoculated with 1×10^6 tumor cells suspended in 50 µl in the fifth mammary fat pad. Two days after inoculation, tumors were intratumorally injected with 100 µl of 1 mM STF-1084 in PBS or with PBS alone. For experiments using STING and mENPP1, 100 µl of 100 µM neutralizing STING or non-binding STING (R237A) and 700 nM mENPP1 or PBS were injected intratumorally.

Alternatively, C57BL/6 mice were inoculated with 5×10^4 E0771 tumor cells suspended in 50 µl in the fifth mammary fat pad. After tumor volume reached 100 ± 20 mm^3, tumors were irradiated with 8 Gy. Two and 4 d after IR, tumors were intratumorally injected with 100 µl of 100 µM neutralizing STING or non-binding STING (R237A).

The next day, the tumor was extracted and incubated in RPMI supplemented with 10% FBS containing 20 µg ml^{-1} DNase I type IV (Sigma-Aldrich) and 1 mg ml^{-1} collagenase from *Clostridium histolyticum* (Sigma-Aldrich) at 37 °C for 30 min. Tumors were passed through a 100-µm cell strainer (Sigma-Aldrich), and red blood cells were lysed with red blood cell lysis buffer (155 mM NH_4Cl, 12 mM $NaHCO_3$ and 0.1 mM EDTA) for 5 min at room temperature. Cells were stained with the Live/Dead Fixable Near-IR Dead Cell staining kit (Thermo Fisher Scientific; 1:1,000 in accordance with the manufacturer's description), Fc blocked for 10 min with TruStain fcX (101320, BioLegend, clone 93; 1:100) and subsequently stained with the following antibodies: CD8α-AF594 (100758, BioLegend, clone 53-6.7; 1:200), CD11c-PE (117308, BioLegend, clone N418; 1:200), CD45-AF700 (103128, BioLegend, clone 30-F11; 1:800) or CD45-BV650 (103151, BioLegend, clone 30-F11; 1:100), CD62L-BV785 (104440, BioLegend, clone MEL-14; 1:200), F4/80-APC (123116, BioLegend, clone BM8; 1:200), granzyme B-AF647 (515406, BioLegend, clone GB11; 1:100), I-A/I-E-FITC (107606, BioLegend, clone M5/114.15.2; 1:800), CD3ε-PerCP-eF710 (46-0033-82, eBioscience, clone eBio500A2; 1:200), CD25-eF450 (48-0251-82, eBioscience, PC61.5; 1:200) and CD103-BUV395 (740238, BD Biosciences, clone M290; 1:400). Caspase activity was detected after red blood cell lysis with the FAM-FLICA Poly Caspase Assay kit (ImmunoChemistry Technologies) according to the manufacturer's description.

Cells were analyzed on an SH800S cell sorter (Sony), an LSR II (BD Biosciences) or an Aurora (Cytek). Data were analyzed with FlowJo v10 software (Treestar) and Prism 7.04 software (GraphPad) for statistical analysis, and statistical significance was assessed by unpaired two-tailed *t* test with Welch's correction.

In vivo imaging. Mice were injected intraperitoneally with 3 mg XenoLight D-luciferin (Perkin Elmer) in 200 µl water and imaged with a Lago X in vivo imaging system (Spectral Instruments Imaging). Object height was set to 1.5 cm, binning to 4 and FStop to 1.2. The exposure time was 120 s. Images were analyzed with aura 2.0.1 software (Spectral Instruments Imaging).

Synthesis of STF-1084. Preparation of dimethyl (*E*)-(2-(1-benzylpiperidin-4-yl) vinyl)phosphonate. Sodium hydride (2.16 g, 54.11 mmol) was carefully added to a stirred solution of bis(dimethoxyphosphoryl)methane (11.42 g, 49.19 mmol) in toluene (100 ml) at room temperature. The reaction mixture was then placed under an atmosphere of nitrogen, and a solution of 1-benzylpiperidine-4-carbaldehyde (10 g, 49.19 mmol) in toluene (50 ml) was slowly added, keeping the temperature below 40 °C. The resulting mixture was left to stir at room temperature for 16 h and then quenched by the addition of aqueous saturated ammonium chloride solution. The organic phase was separated, washed with brine, dried ($MgSO_4$) and evaporated to dryness. Chromatography (120 g SiO_2; 5–100% gradient of ethyl acetate in hexanes) provided dimethyl (*E*)-(2-(1-benzylpiperidin-4-yl)vinyl) phosphonate (6.2 g, 16%) as a colorless oil.

LC–MS (*m*/*z*): 309.8 $[M+H]^+$

^{1}H NMR (500 MHz, chloroform-*d*): δ 7.47–7.21 (m, 5H), 6.86–6.73 (m, 1H), 5.65–5.53 (m, 1H), 3.75 (s, 3H), 3.70 (s, 3H), 3.52 (s, 2H), 2.98–2.87 (m, 2H), 2.22–2.11 (m, 1H), 2.09–1.99 (m, 2H), 1.79–1.70 (m, 2H), 1.54–1.44 (m, 2H)

Preparation of dimethyl (2-(piperidin-4-yl)ethyl)phosphonate. To a mixture of dimethyl (*E*)-(2-(1-benzylpiperidin-4-yl)vinyl)phosphonate (6.2 g, 20.0 mmol) in ethanol (80 ml) was added $Pd(OH)_2$/C (0.5 g). The mixture was exchanged with hydrogen gas three times and stirred under hydrogen balloon at room temperature for 12 h. The mixture was filtered through Celite and evaporated to dryness to give 4.4 g (100% yield with ~90% purity) of dimethyl (2-(piperidin-4-yl)ethyl) phosphonate as colorless oil.

^{1}H NMR (500 MHz, chloroform-*d*): δ 3.75 (s, 3H), 3.73 (s, 3H), 3.08 (dt, J = 12.5, 3.2 Hz, 2H), 2.58 (td, J = 12.2, 2.5 Hz, 2H), 1.80–1.60 (m, 4H), 1.60–1.50 (m, 2H), 1.38 (m, 1H), 1.11 (qd, J = 12.1, 4.0 Hz, 2H)

Preparation of dimethyl (2-(1-(6,7-dimethoxyquinazolin-4-yl)piperidin-4-yl)ethyl) phosphonate. Diisopropylethylamine (0.6 g, 8.9 mmol) was added to a mixture of dimethyl (2-(piperidin-4-yl)ethyl)phosphonate (1.1 g, 4.9 mmol) and 4-chloro-6,7-dimethoxy-quinazoline (1.0 g, 4.5 mmol) in isopropyl alcohol (20 ml). After stirring at 90 °C for 3 h, the reaction mixture was cooled and evaporated to dryness. Purification of silica gel (5% methanol in dichloromethane) provided dimethyl (2-(1-(6,7-dimethoxyquinazolin-4-yl)piperidin-4-yl)ethyl)phosphonate (755 mg, 37%) as oil.

LC–MS (*m*/*z*): 410.25 $[M+H]^+$

^{1}H NMR (500 MHz, $CDCl_3$): δ 8.65 (s, 1H), 7.23 (s, 1H), 7.09 (s, 1H), 4.19 (dq, J = 14.0, 2.9, 2.4 Hz, 2H), 4.02 (s, 3H), 3.99 (s, 3H), 3.77 (s, 3H), 3.75 (s, 3H), 3.05 (td, J = 12.8, 2.3 Hz, 2H), 1.93–1.77 (m, 4H), 1.67 (ddd, J = 14.1, 9.5, 5.9 Hz, 3H), 1.46 (qd, J = 12.2, 3.7 Hz, 2H)

Preparation of dimethyl (2-(1-(6,7-dimethoxyquinazolin-4-yl)piperidin-4-yl) ethyl)phosphonic acid hydrogen bromide salt (STF-1084). Bromotrimethylsilane (3.67 g, 24 mmol) was added to a cooled solution of dimethyl (2-(1-(6,7-dimethoxyquinazolin-4-yl)piperidin-4-yl)ethyl)phosphonate (3.25 g, 7.94 mmol) in chloroform (60 ml) that was cooled by an ice bath. The reaction mixture was allowed to warm to room temperature and after 90 min was quenched by the addition of methanol (20 ml). The mixture was evaporated to dryness under reduced pressure and then solvated in methanol (100 ml). The reaction mixture was concentrated to half volume, filtered to remove precipitate and then evaporated to dryness. The residue was crystalized with dichloromethane, filtered

and dried under vacuum to give dimethyl (2-(1-(6,7-dimethoxyquinazolin-4-yl) piperidin-4-yl)ethyl)phosphonic acid (2.1 g, 69%).

LC–MS (*m/z*): 381.8 $[M+H]^+$

^{1}H NMR (500 MHz, DMSO-d_6): δ 8.77 (s, 1H), 7.34 (s, 1H), 7.23 (s, 1H), 4.71 (d, J = 13.1 Hz, 2H), 3.99 (s, 3H), 3.97 (s, 3H), 3.48 (t, J = 12.7 Hz, 2H), 3.18 (s, 1H), 1.97–1.90 (m, 2H), 1.62–1.43 (m, 4H), 1.40–1.27 (m, 2H)

^{13}C NMR (126 MHz, methanol-d_4): δ 162.70, 158.44, 150.72, 147.43, 138.54, 107.54, 107.34, 100.15, 57.32, 56.98, 49.54, 37.44, 37.32, 33.20, 30.20 (d, $^1J_{C\text{-}P}$ = 3.78 Hz), 25.85, 24.74

Synthesis of STF-1623. (2-(1-(8-methoxyquinazolin-4-yl)piperidin-4-yl) ethyl)phosphonic acid (STF-1623) was prepared according to the same synthetic procedure as STF-1084, by using 4-chloro-8-methoxyquinazoline instead of 4-chloro-6,7-dimethoxyquinazoline in the preparation of dimethyl (2-(1-(8-dimethoxyquinazolin-4-yl)piperidin-4-yl)ethyl)phosphonate.

LC–MS (*m/z*): 352.1 $[M+H]^+$

^{1}H NMR (400 MHz, DMSO-d_6): δ 8.62 (s, 1H), 7.63–7.53 (m, 3H), 6.65 (d, J = 12.4 Hz, 2H), 4.02 (s, 3H), 3.39–3.36 (m, 2H), 1.92 (m, 2H), 1.58–1.56 (m, 1H), 1.54–1.45 (m, 4H), 1.35–1.30 (m, 2H)

^{13}C NMR (126 MHz, D_2O): δ 162.77, 152.41, 150.66, 139.37, 125.78, 116.72, 115.40, 111.97, 55.61, 49.96, 36.26, 36.13, 31.35, 29.77 (d, $^1J_{C\text{-}P}$ = 3.78 Hz), 25.85, 24.79

Statistics and reproducibility. For treatment of established tumors in mice, power calculations were performed to estimate that cohorts of nine mice were needed. Calculations were based on a pilot study using a two-sided significance level of 0.05 and power of 0.8, determined by Mann–Whitney *U* test. The effect size of 1.9 and power calculations were performed with G*Power 3.1. Mice from different treatment groups were randomly housed together in each cage to eliminate cage effects. The experimenter was blinded to group allocation and analysis. No data were excluded from the analyses.

For all other experiments, no statistical method was used to predetermine sample sizes. For flow cytometry analysis of tumors, sample sizes were chosen to be 2–6 mice. For in vitro and cell culture experiments, sample sizes were chosen to be 2–3 biological replicates except in Figs. 2e–g and 5e, and Extended Data Figs. 2b, 3d and 10d, where titrations or time courses were performed and the sample size was chosen to be 1, with two technical replicates. The experiments were not randomized. The experimenter was not blinded to group allocation. No data were excluded from the analyses.

Either independent experiments (experiments repeated with identical assay conditions) or independent validations (experiments repeated with similar, but not identical, conditions that validated results overall, but not precisely) were performed as indicated in the figure legends. Data from independent validations are shown in Supplementary Figs. 1–5 as indicated. For data shown in Figs. 1b,f, 2d, 3e,f,j (in cell assays) and 4a–c (Neuro-2a, MDA-MB-231, HeLa), and Extended Data Figs. 3f, 4a,e and 10b,d,f (in cell assays), the experiment was performed once. The results were supported by orthogonal experiments, as indicated in the figure legends.

Reporting Summary. Further information on research design is available in the Nature Research Reporting Summary linked to this article.

Data availability

The *ENPP1* mRNA expression data were derived from the TCGA Research Network: http://cancergenome.nih.gov/. Source data for Figs. 1–5 and Extended Data Figs. 1–5, 7, 9 and 10 are provided with the paper. Independent validators for Figs. 1–5 are provided as Supplementary Figs. 1–5. All other data that support the findings of this study are available from the corresponding author upon request.

Received: 27 September 2019; Accepted: 15 January 2020;
Published online: 24 February 2020

References

1. Wu, J. et al. Cyclic GMP-AMP is an endogenous second messenger in innate immune signaling by cytosolic DNA. *Science* **339**, 826–830 (2013).
2. Sun, L., Wu, J., Du, F., Chen, X. & Chen, Z. J. Cyclic GMP-AMP synthase is a cytosolic DNA sensor that activates the type I interferon pathway. *Science* **339**, 786–791 (2013).
3. Li, X.-D. et al. Pivotal roles of cGAS–cGAMP signaling in antiviral defense and immune adjuvant effects. *Science* **341**, 1390–1394 (2013).
4. Barber, G. N. STING: infection, inflammation and cancer. *Nat. Rev. Immunol.* **15**, 760–770 (2015).
5. Ishikawa, H., Ma, Z. & Barber, G. N. STING regulates intracellular DNA-mediated, type I interferon-dependent innate immunity. *Nature* **461**, 788–792 (2009).
6. Ahn, J., Gutman, D., Saijo, S. & Barber, G. N. STING manifests self DNA-dependent inflammatory disease. *Proc. Natl Acad. Sci. USA* **109**, 19386–19391 (2012).
7. Woo, S. R. et al. STING-dependent cytosolic DNA sensing mediates innate immune recognition of immunogenic tumors. *Immunity* **41**, 830–842 (2014).
8. Ishikawa, H. & Barber, G. N. STING is an endoplasmic reticulum adaptor that facilitates innate immune signalling. *Nature* **455**, 674–678 (2008).
9. Ablasser, A. et al. Cell intrinsic immunity spreads to bystander cells via the intercellular transfer of cGAMP. *Nature* **503**, 530–534 (2013).
10. Patel, S. J., King, K. R., Casali, M. & Yarmush, M. L. DNA-triggered innate immune responses are propagated by gap junction communication. *Proc. Natl Acad. Sci. USA* **106**, 12867–12872 (2009).
11. Patel, S. J. et al. Gap junction inhibition prevents drug-induced liver toxicity and fulminant hepatic failure. *Nat. Biotechnol.* **30**, 179–183 (2012).
12. Chen, Q. et al. Carcinoma-astrocyte gap junctions promote brain metastasis by cGAMP transfer. *Nature* **533**, 493–498 (2016).
13. Gentili, M. et al. Transmission of innate immune signaling by packaging of cGAMP in viral particles. *Science* **349**, 1232–1236 (2015).
14. Bridgeman, A. et al. Viruses transfer the antiviral second messenger cGAMP between cells. *Science* **349**, 1228–1232 (2015).
15. Marcus, A. et al. Tumor-derived cGAMP triggers a STING-mediated interferon response in non-tumor cells to activate the NK cell response. *Immunity* **49**, 754–763 (2018).
16. Li, L. et al. Hydrolysis of 2′3′-cGAMP by ENPP1 and design of nonhydrolyzable analogs. *Nat. Chem. Biol.* **10**, 1043–1048 (2014).
17. Gao, P. et al. Structure–function analysis of STING activation by c[G(2′,5′) pA(3′,5′)p] and targeting by antiviral DMXAA. *Cell* **154**, 748–762 (2013).
18. Corrales, L. et al. Direct activation of STING in the tumor microenvironment leads to potent and systemic tumor regression and immunity. *Cell Rep.* **11**, 1018–1030 (2015).
19. Ritchie, C., Cordova, A. F., Hess, G. T., Bassik, M. C. & Li, L. SLC19A1 is an importer of the immunotransmitter cGAMP. *Mol. Cell* **75**, 372–381 (2019).
20. Luteijn, R. D. et al. SLC19A1 transports immunoreactive cyclic dinucleotides. *Nature* **573**, 434–438 (2019).
21. Jønsson, K. L. et al. IFI16 is required for DNA sensing in human macrophages by promoting production and function of cGAMP. *Nat. Commun.* **8**, 1–17 (2017).
22. Gao, D. et al. Activation of cyclic GMP-AMP synthase by self-DNA causes autoimmune diseases. *Proc. Natl Acad. Sci. USA* **112**, E5699–E5705 (2015).
23. Sun, W. et al. ERIS, an endoplasmic reticulum IFN stimulator, activates innate immune signaling through dimerization. *Proc. Natl Acad. Sci. USA* **106**, 8653–8658 (2009).
24. Belli, S., van Driel, I. & Goding, J. Identification and characterization of a soluble form of the plasma cell membrane glycoprotein PC-1. *Eur. J. Biochem.* **217**, 421–428 (1993).
25. Mackenzie, K. J. et al. cGAS surveillance of micronuclei links genome instability to innate immunity. *Nature* **548**, 461–465 (2017).
26. Harding, S. M. Mitotic progression following DNA damage enables pattern recognition within micronuclei. *Nature* **548**, 466–470 (2017).
27. Bakhoum, S. F. et al. Chromosomal instability drives metastasis through a cytosolic DNA response. *Nature* **553**, 467–472 (2018).
28. Zhou, W. et al. Structure of the human cGAS–DNA complex reveals enhanced control of immune surveillance. *Cell* **174**, 300–311 (2018).
29. Zhao, Y. J., Lam, C. M. C. & Lee, H. C. The membrane-bound enzyme CD38 exists in two opposing orientations. *Sci. Signal.* **5**, ra67 (2012).
30. Patel, S. D. et al. Quinazolin-4-piperidin-4-methyl sulfamide PC-1 inhibitors: alleviating hERG interactions through structure based design. *Bioorganic Med. Chem. Lett.* **19**, 3339–3343 (2009).
31. Shayhidin, E. E. et al. Quinazoline-4-piperidine sulfamides are specific inhibitors of human NPP1 and prevent pathological mineralization of valve interstitial cells. *Br. J. Pharmacol.* **172**, 4189–4199 (2015).
32. Hatch, E. M., Fischer, A. H., Deerinck, T. J. & Hetzer, M. W. Catastrophic nuclear envelope collapse in cancer cell micronuclei. *Cell* **154**, 47 (2013).
33. Bakhoum, S. F. et al. Numerical chromosomal instability mediates susceptibility to radiation treatment. *Nat. Commun.* **6**, 1–10 (2015).
34. Dou, Z. et al. Cytoplasmic chromatin triggers inflammation in senescence and cancer. *Nature* **550**, 402–406 (2017).
35. Böttcher, J. P. & Reis e Sousa, C. The role of type 1 conventional dendritic cells in cancer immunity. *Trends Cancer* **4**, 784–792 (2018).
36. Rutsch, F. et al. PC-1 nucleoside triphosphate pyrophosphohydrolase deficiency in idiopathic infantile arterial calcification. *Am. J. Pathol.* **158**, 543–554 (2001).
37. Deng, L. et al. STING-dependent cytosolic DNA sensing promotes radiation-induced type I interferon-dependent antitumor immunity in immunogenic tumors. *Immunity* **41**, 543–852 (2014).
38. Yang, H., Wang, H., Ren, J., Chen, Q. & Chen, Z. J. cGAS is essential for cellular senescence. *Proc. Natl Acad. Sci. USA* **114**, E4612–E4620 (2017).
39. Lau, W. M. et al. Enpp1: a potential facilitator of breast cancer bone metastasis. *PLoS One* **8**, 1–5 (2013).
40. Takahashi, R. U. et al. Loss of microRNA-27b contributes to breast cancer stem cell generation by activating ENPP1. *Nat. Commun.* **6**, 1–15 (2015).
41. Umar, A. et al. Identification of a putative protein profile associated with tamoxifen therapy resistance in breast cancer. *Mol. Cell Proteomics* **8**, 1278–1294 (2009).

42. Cerami, E. et al. The cBio cancer genomics portal: an open platform for exploring multidimensional cancer genomics data. *Cancer Discov.* **2**, 401–404 (2012).
43. Gao, J. et al. Integrative analysis of complex cancer genomics and clinical profiles using the cBioPortal. *Sci. Signal.* **6**, pl1 (2013).
44. Negrini, S., Gorgoulis, V. G. & Halazonetis, T. D. Genomic instability—an evolving hallmark of cancer. *Nat. Rev. Mol. Cell Biol.* **11**, 220–228 (2010).
45. Bakhoum, S. F. & Cantley, L. C. The multifaceted role of chromosomal instability in cancer and its microenvironment. *Cell* **174**, 1347–1360 (2018).
46. Konno, H., Konno, K. & Barber, G. N. Cyclic dinucleotides trigger ULK1 (ATG1) phosphorylation of STING to prevent sustained innate immune signaling. *Cell* **155**, 688–698 (2013).
47. Xu, M. M. et al. Dendritic cells but not macrophages sense tumor mitochondrial DNA for cross-priming through signal regulatory protein A signaling. *Immunity* **47**, 363–373 (2017).
48. Vanpouille-Box, C. et al. DNA exonuclease Trex1 regulates radiotherapy-induced tumour immunogenicity. *Nat. Commun.* **8**, 15618 (2017).
49. Lau, L., Gray, E. E., Brunette, R. L. & Stetson, D. B. DNA tumor virus oncogenes antagonize the cGAS–STING DNA-sensing pathway. *Science* **350**, 568–571 (2015).
50. Vilalta, M., Rafat, M., Giaccia, A. J. & Graves, E. E. Recruitment of circulating breast cancer cells is stimulated by radiotherapy. *Cell Rep.* **8**, 402–409 (2014).
51. Kato, K. et al. Expression, purification, crystallization and preliminary X-ray crystallographic analysis of Enpp1. *Acta Crystallogr. Sect. F Struct. Biol. Cryst. Commun.* **68**, 778–782 (2012).
52. Amend, S. R., Valkenburg, K. C. & Pienta, K. J. Murine hind limb long bone dissection and bone marrow isolation. *J. Vis. Exp.* https://doi.org/10.3791/53936 (2016).
53. Sanjana, N. E., Shalem, O. & Zhang, F. Improved vectors and genome-wide libraries for CRISPR screening. *Nat. Methods* **11**, 783–784 (2014).
54. Kato, K. et al. Crystal structure of Enpp1, an extracellular glycoprotein involved in bone mineralization and insulin signaling. *Proc. Natl Acad. Sci. USA* **109**, 16876–16881 (2012).

Acknowledgements

This work is dedicated to T. Mitchison to celebrate his 60th birthday and his remarkable achievements in understanding biochemical mechanisms of the cell. He taught L. Li the power of definitive experiments. We thank the following people (all affiliated with Stanford) for their help: the Stanford Small Animal Imaging Facility, S. Ergun for [^{35}S] cGAMP, C. Patel for specificity assays, F. Sunden for enzyme assays, R. Stabler for chemical synthesis, N. Weng for protein purification, and C. Walsh, D. Herschlag and all members of the Li laboratory for helpful discussions. Flow cytometry analysis for this project was performed on instruments in the Stanford Shared FACS Facility. Data were collected on an instrument in the Shared FACS Facility obtained using NIH S10 Shared Instrument Grant S10RR027431-01. This research was supported by NIH grant 5F31CA239510 (J.A.C), a Xu Family Foundation Stanford Interdisciplinary Graduate Fellowship affiliated with Stanford ChEM-H (J.A.C.), NIH grant DP2CA228044 (L.L.), Department of Defense grant W81XWH-18-1-0041 (L.L.), NSF GRFP DGE1656518 (J.A.B.), U19AI109662 (J.S.G.), R01CA197136 and S10OD018208 (E.E.G.) and K99CA201304 (M.R.).

Author contributions

J.A.C., V.B., K.E.S., M.S. and L.L. designed the study. J.A.C., V.B., K.E.S., K.C.N., G.S., J.A.B., M.R. and L.L. performed experiments and analyzed data. R.E. performed statistical analysis. J.A.C., V.B. and L.L. wrote the manuscript. J.S.G. supervised K.C.N.; E.E.G. supervised M.R. and R.E. All authors discussed the findings and commented on the manuscript.

Competing interests

M.S. and L.L. are scientific cofounders of Angarus Therapeutics, which has exclusive licensing rights to patent PCT/US2018/50018. J.A.C., V.B., K.E.S., M.S. and L.L. are inventors on patent PCT/US2018/50018.

Additional information

Supplementary information is available for this paper at https://doi.org/10.1038/s43018-020-0028-4.

Correspondence and requests for materials should be addressed to L.L.

Reprints and permissions information is available at www.nature.com/reprints.

Publisher's note Springer Nature remains neutral with regard to jurisdictional claims in published maps and institutional affiliations.

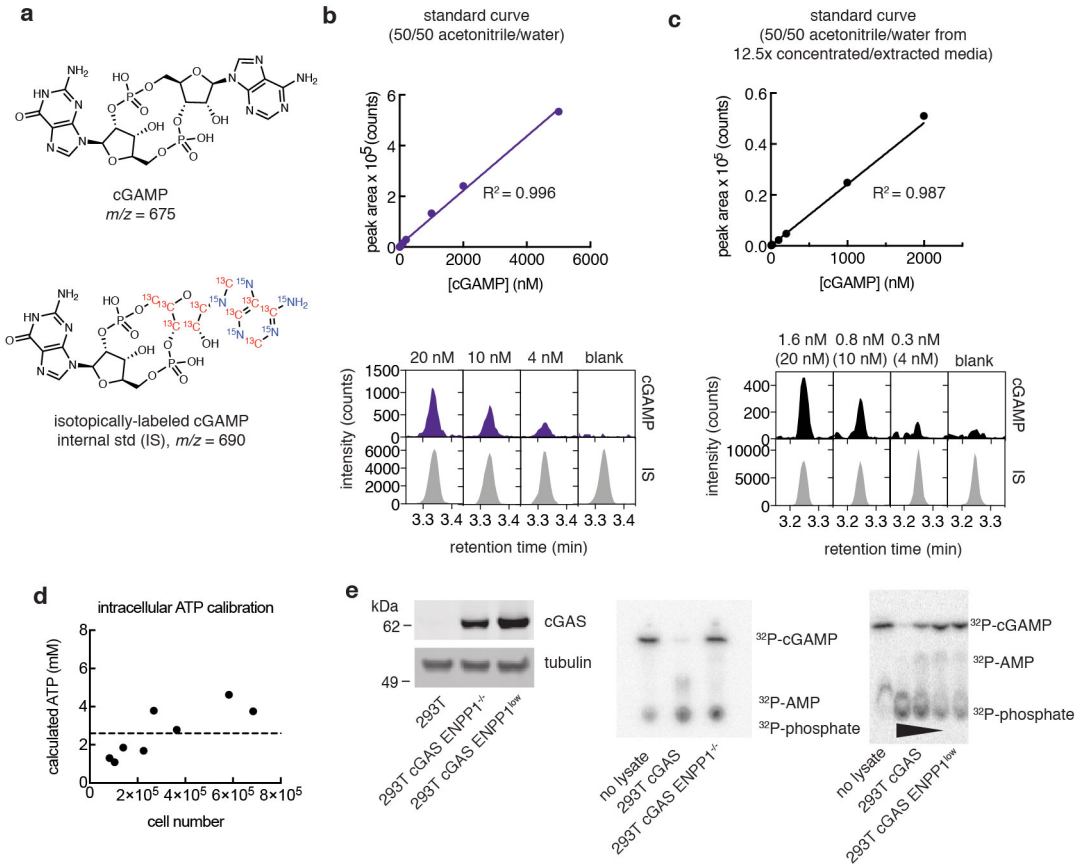

Extended Data Fig. 1 | Measuring cGAMP in 293T cGAS cell lines by LC-MS/MS. a, Chemical structures of cGAMP (top) and single isotopically-labeled cGAMP (bottom) used as an internal standard at a concentration of 0.5-1 μM. **b-c**, Full (7-8 point) standard curves and LC traces of lowest cGAMP standards in 50/50 acetonitrile/water spiked in directly (LOQ = 4 nM) (**b**) or after concentrating and extracting 12.5x from complete cell culture media (LOQ = 0.3 nM from original sample, 4 nM in concentrated sample) (**c**). IS = internal standard. R^2 = coffecient of determination, determined after linear least squares regression with $1/Y^2$ weighting. Data are from 1 experiment, representative of (**b**) 64 independent experiments and (**c**) 13 independent experiments. **d**, Calibration of cell number to ATP concentration measured by LC-MS/MS. Data are from one experiment, representative of two independent experiments, 8 individual cell culture replicates are plotted. **e**, cGAS expression of 293T, 293T cGAS ENPP1$^{-/-}$, and 293T cGAS ENPP1^{low} cell lines analyzed by western blot (left; full scan of blot available in Source Data). ENPP1 hydrolysis activity of ^{32}P-cGAMP in whole cell lysates from 1 million each of 293T cGAS, 293T cGAS ENPP1$^{-/-}$, and 293T cGAS ENPP1^{low} cells, measured by TLC and autoradiography (right). Data are from 1 experiment, representative of 5 independent experiments.

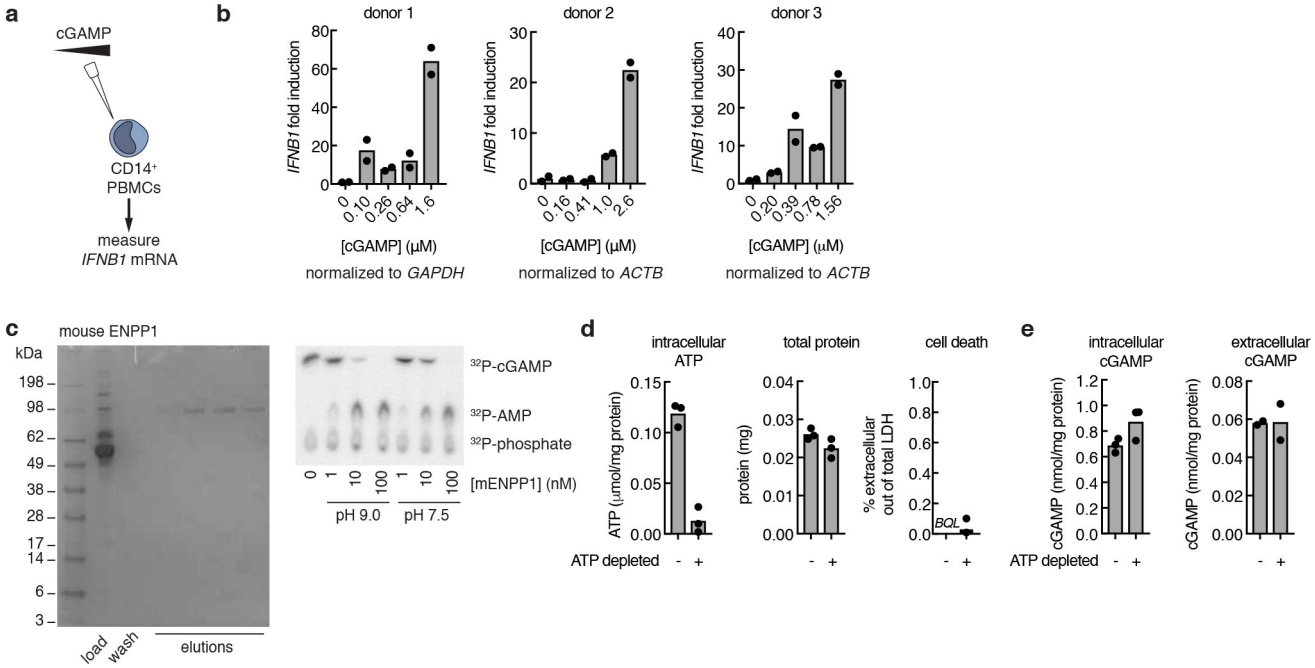

Extended Data Fig. 2 | Development of assays to investigate the mechanism of cGAMP export. a, Schematic of experiment for **b**. CD14+ PMBCs were stimulated with increasing concentrations of extracellular cGAMP for 16 h. **b**, *IFNB1* mRNA levels were normalized to indicated gene and fold induction was calculated relative to untreated CD14+ cells. Each donor was performed as one independent experiment; 2 qPCR replicates are plotted with a bar representing the mean. **c**, Coomassie gel of recombinant mouse ENPP1 purified from media; elution fractions were pooled before use (left). ^{32}P-cGAMP degradation by mouse ENPP1 analyzed by TLC (right). Data are representative of 10 independent experiments. **d–e**, 293T cGAS ENPP1^{low} cells were incubated with serum-free ATP depletion media (no glucose, 6 mM 2-deoxy-D-glucose, 5 mM NaN_3) or serum-free complete media for 1 hour. Levels of analytes were measured: (**d**) ATP by LC-MS/MS, total protein by BCA, cell death by extracellular lactate dehydrogenase activity, and (**e**) cGAMP by LC-MS/MS. *BQL* = below quantification limit. Data are from 1 experiment; 3 cell culture replicates are plotted (except for extracellular cGAMP, where 2 cell culture replicates are plotted). ATP data are representative of 3 independent validations (shown in Supplementary Fig. 5).

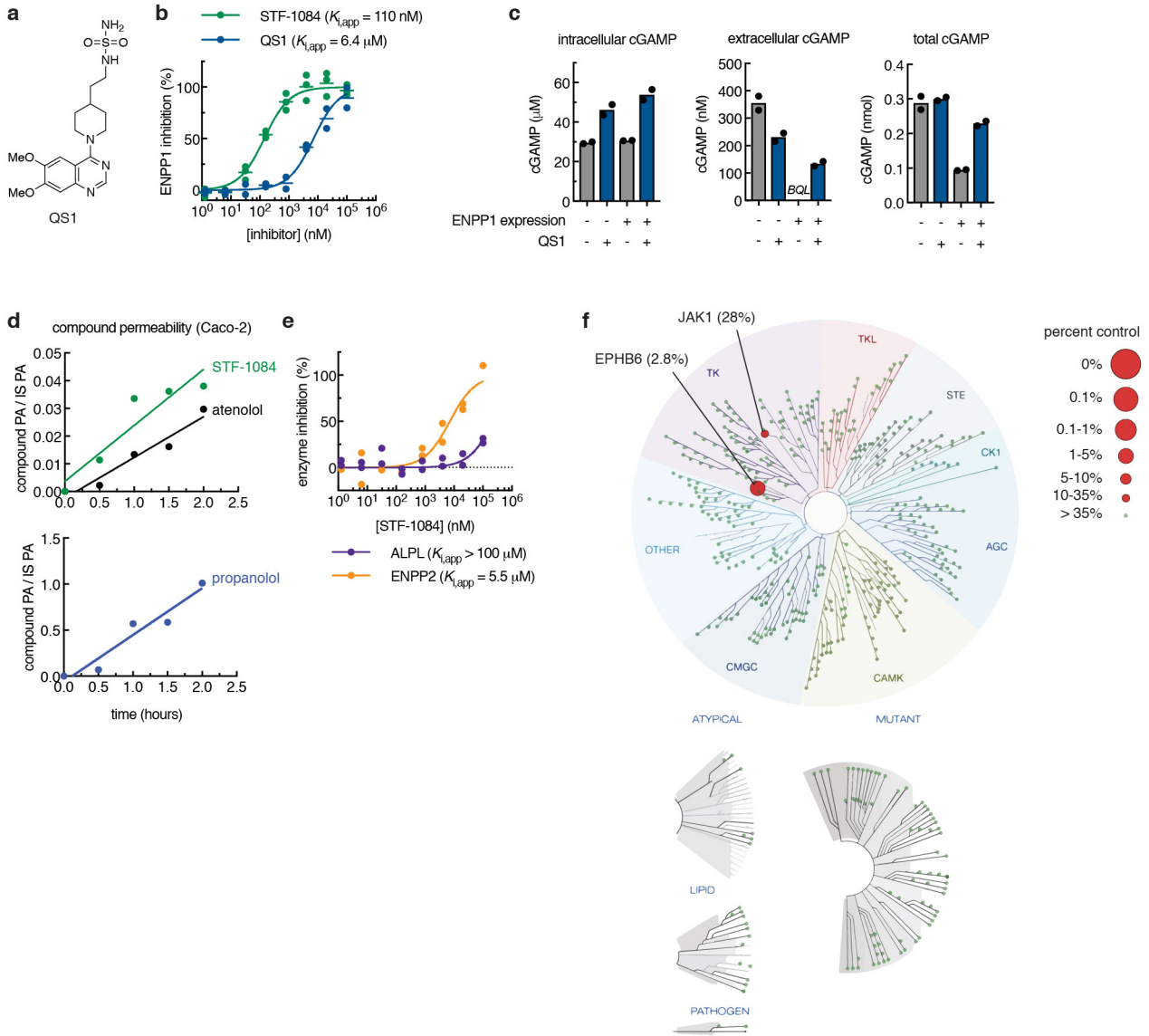

Extended Data Fig. 3 | Characterization of ENPP1 inhibitors QS1 and STF-1084. a, Structure of QS1. **b**, Inhibition by QS1 (compared to STF-1084, replotted from Fig. 3e). in vitro (^{32}P-cGAMP TLC assay, pH 7.5, purified mouse ENPP1): $K_{i,app}$ = 6.4 μM, 2 independent experiments are plotted with a bar representing the mean. **c**, Intracellular, extracellular, and total cGAMP for 293T cGAS ENPP1$^{-/-}$ cells transfected with pcDNA6 (empty or containing human *ENPP1*) and treated ± QS1 after 24 hours. Data are from 1 experiment, representative of 2 independent validations; 2 cell culture replicates are plotted with a bar representing the mean. **d**, Permeability of compounds in Caco-2 assay. PA = peak area, IS = internal standard. Compounds were incubated on the apical side of a Caco-2 monolayer for 2 hours. Compound concentration on the basolateral side was monitored by LC-MS/MS. Apparent permeability rates (P_{app}) were calculated from the slope. Data are representative of 2 independent experiments; single points are plotted. **e**, Inhibitory activity of STF-1084 against alkaline phosphatase (ALPL) and ENPP2. Data are from 1 experiment, representative of 2 independent validations; 2 reaction replicates are plotted, except for ENPP2 100 uM and 32 nM, where 1 point is plotted. **f**, Kinome interaction map (468 kinases tested) for STF-1084 depicting kinase inhibition as a percent of control. Data visualized with the TREEspot Software Tool and reprinted with permission from KINOMEscan, a division of DiscoveRx Corporation. ©DiscoveRX Corporation 2010.

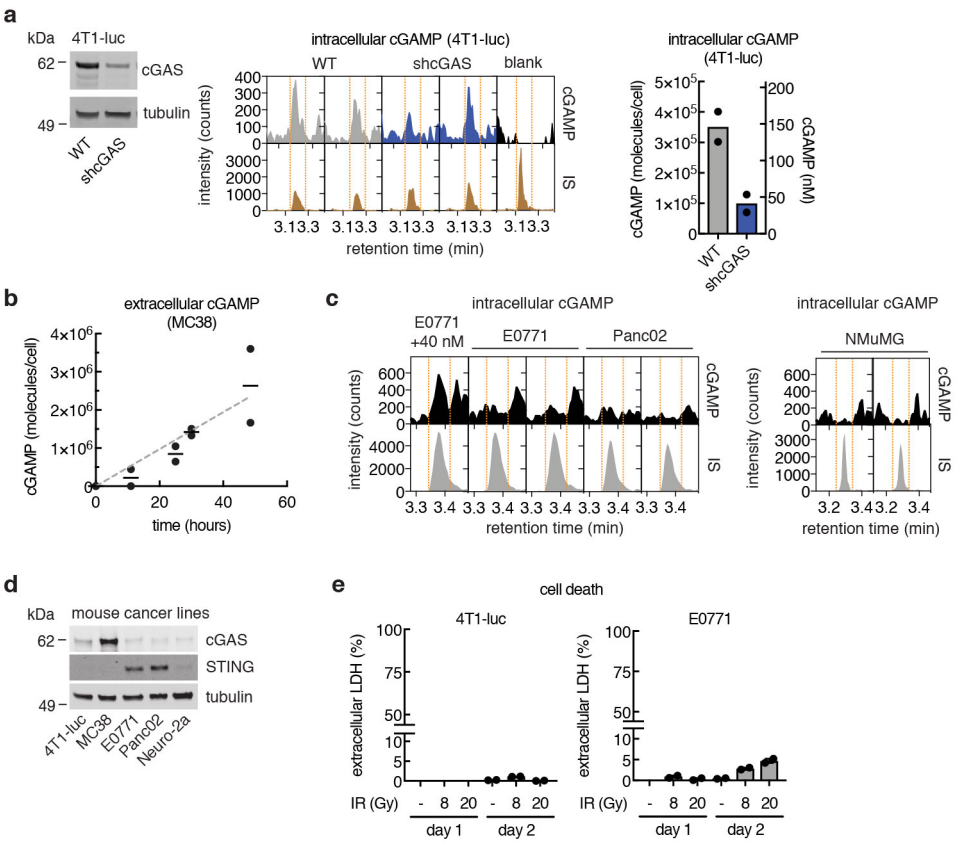

Extended Data Fig. 4 | Intracellular and extracellular cGAMP from cancer cell lines. a, cGAS expression of 4T1-luc WT and 4T1-luc shcGAS analyzed by western blot (full scan of blot available in Source Data). Intracellular cGAMP (chromatograms and quantification displayed) in 4T1-luc WT and shcGAS cells without exogenous stimulation. Concentration reported in units of molecules/cell and nM (estimated using cell volume = 4 pL). IS = internal standard. Data are from 1 experiment; 2 cell culture replicates are plotted. **b**, Extracellular cGAMP produced by MC38 cells over 48 hours. At time 0, cells were refreshed with media supplemented with 50 μM STF-1084. Line depicts linear regression. Data are from one experiment representative of two independent validations; 2 cell culture replicates are plotted with a bar representing the mean. **c**, Chromatograms for E0771, Panc02, and NMuMG cell lysate from LC-MS/MS. E0771 cell lysate was spiked with 40 nM cGAMP to determine limit of quantification. IS = internal standard. Data are representative of 2 independent validations. **d**, cGAS and STING expression of 4T1-luc, MC38, E0771, Panc02, and Neuro-2a cell lines analyzed by western blot (full scan of blot available in Source Data). Data are representative of 3 independent validations. **e**, Cell viability of cancer cell lines 4T1-luc and E0771 measured by lactate dehydrogenase extracellular activity compared to intracellular activity. At time 0, cells were left untreated or treated with IR (8 Gy or 20 Gy) and refreshed with media supplemented with 50 μM STF-1084. Data are from 1 experiment representative of two independent validations; 2 cell culture replicates are plotted with a bar representing the mean.

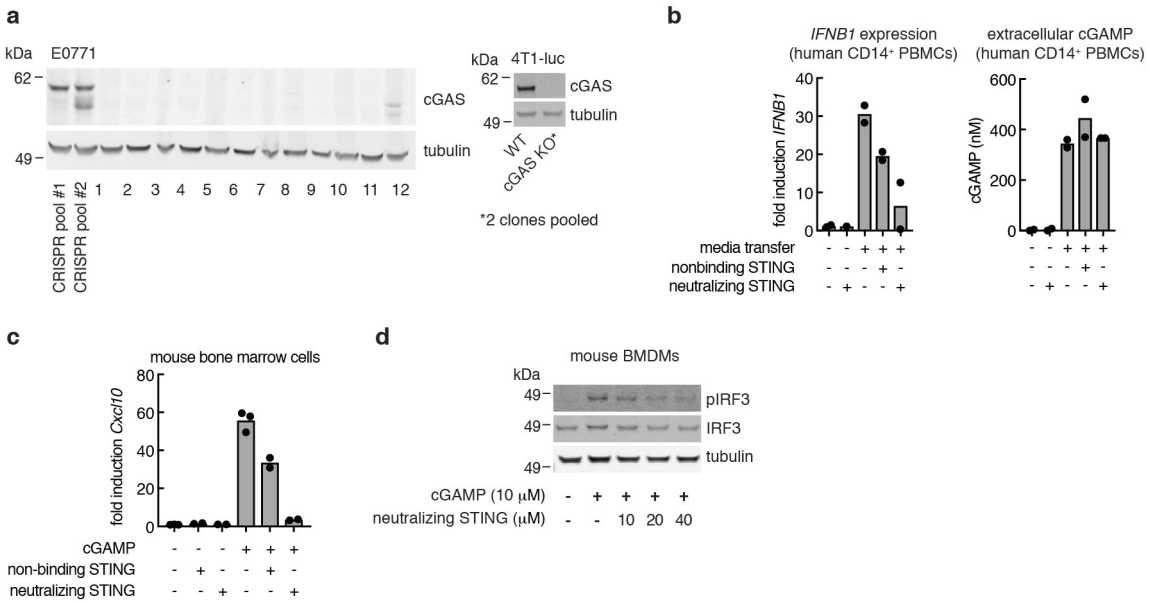

Extended Data Fig. 5 | Validation of *Cgas*$^{-/-}$ cell lines and tools to neutralize extracellular cGAMP. a, E0771 (left) and 4T1-luc (right) *Cgas*$^{-/-}$ cells subcloned from CRISPR knockout pools (full scan of blot available in Source Data). Data are representative of two independent validations. Six E0771 *Cgas*$^{-/-}$ subclones (1, 2, 4, 6, 8, and 9) were pooled before injection into mice. Two 4T1-luc *Cgas*$^{-/-}$ subclones were pooled before injection into mice. **b**, 293T cGAS ENPP1^{low} cells were transfected with empty pcDNA6 (0.5 μg/mL) and incubated for 24 hours. Conditioned media was treated with nonbinding or neutralizing STING (1 hour pretreatment) and then incubated with CD14$^+$ PBMCs for 16 h. Extracellular cGAMP measured by LC-MS/MS and *IFNB1* expression (mRNA levels were normalized to *CD14* and fold induction calculated relative to untreated CD14$^+$ cells). Data are from 1 experiment (supported by data in Fig. 5e and Extended Data Fig. 5c,d); 2 cell culture replicates are plotted. **c**, *Cxcl10* mRNA fold induction (normalized to *Actb* and untreated cells) in primary mouse bone marrow cells treated with 20 μM cGAMP in the presence of neutralizing or non-binding STING (100 μM) for 16 h. Data are from 1 experiment (supported by data in Fig. 5e and Extended Data Fig. 5b,d); cell culture replicates plotted are (from left to right) 3, 2, 2, 3, 2, 2. **d**, Mouse bone marrow-derived macrophages were incubated with 10 uM cGAMP and indicated concentrations of neutralizing STING protein for 2 hours. Levels of pIRF3 and IRF3 were analyzed by western blotting. Data are from 1 experiment (supported by data in Fig. 5e and Extended Data Fig. 5b,c) (full scan of blot available in Source Data).

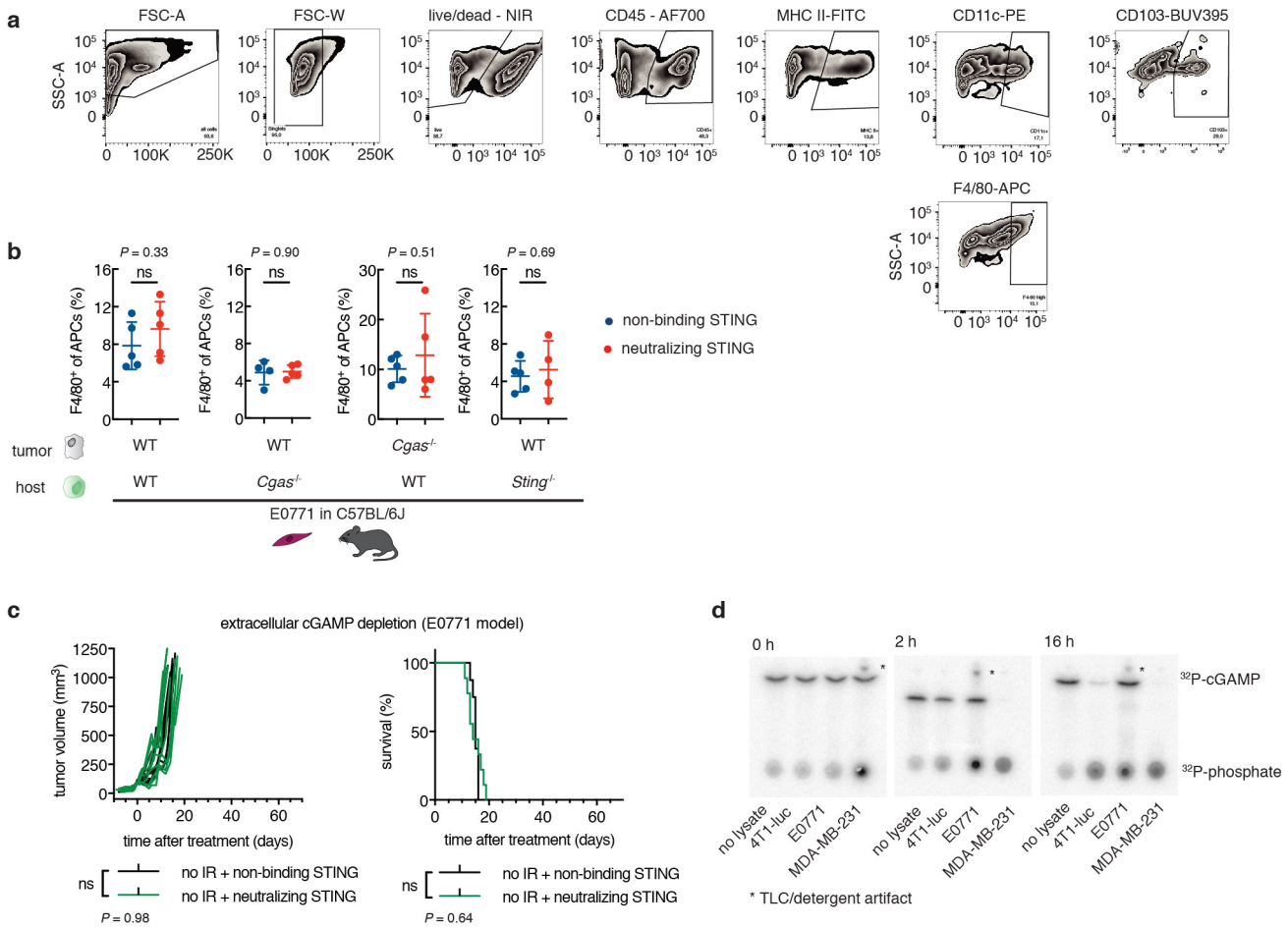

Extended Data Fig. 6 | FACS analysis and tumor growth following extracellular cGAMP depletion in untreated tumors. a, FACS gating scheme for experiments in Fig. 5f–i, Fig. 7b, c and Extended Data Fig. 6b. **b**, WT or *Cgas*$^{-/-}$ E0771 cells (1x10^6) were orthotopically injected into WT, *Cgas*$^{-/-}$ or *Sting1*$^{-/-}$ C57BL/6 J mice on day 0. Neutralizing STING or non-binding STING was intratumorally injected on day 2. Sample sizes of *n* mice, from left to right (non-binding STING, neutralizing STING): *n* = (5, 5); (4, 5); (5, 5); (5, 4). Mean ± SD, unpaired two-tailed *t* test with Welch's correction. **c**, Established E0771 tumors (100 ± 20 mm^3) were injected with non-binding (*n* = 8 mice) or neutralizing STING (*n* = 9 mice) every other day for the duration of the experiment. Tumor volumes for individual mice are shown. *P* value for tumor volume determined by pairwise comparisons using post hoc tests with a Tukey adjustment and for Kaplan Meier curve determined using the Log-rank Mantel-Cox test. **d**, ENPP1 activity in 4T1-luc, E0771, and MDA-MB-231 cells using the ^{32}P-cGAMP degradation assay. Data from 1 experiment, representative of 3 independent validations

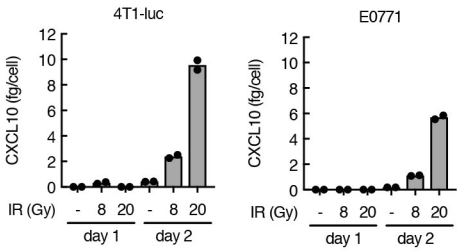

Extended Data Fig. 7 | Cytokine production in cancer cell lines treated with ionizing radiation. CXCL10 production by cancer cell lines 4T1-luc and E0771 measured by ELISA. At time 0, cells were left untreated or treated with IR (8 Gy or 20 Gy) and refreshed with media supplemented with 50 μM STF-1084. Data are from 1 experiment, representative of 2 independent validations; 2 cell culture replicates are plotted with a bar representing the mean.

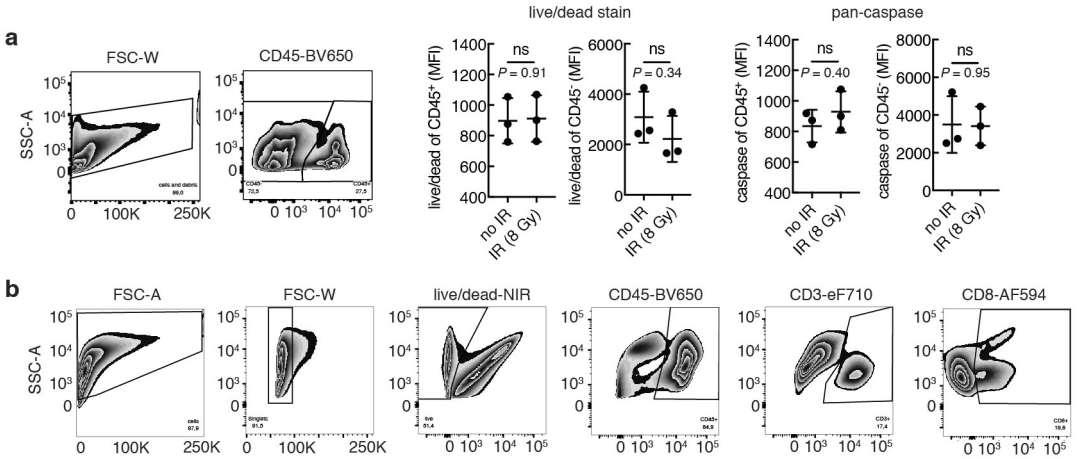

Extended Data Fig. 8 | FACS analysis of tumors treated with ionizing radiation. a, FACS gating scheme for live dead analysis in established tumors. E0771 cells (5x10^4) were orthotopically injected into WT C57BL/6 J mice. The tumors were treated with IR (8 Gy) when they reached 100 ± 20 mm^3 and harvested and analyzed by FACS 24 h after IR. For caspase activity, a single cell suspension was incubated for 1 h with the FAM-FLICA Poly Caspase substrate before FACS stain and analysis. Mean ± SD, unpaired two-tailed *t* test with Welch's correction. **b**, FACS gating scheme for experiments in Fig. 6c,d

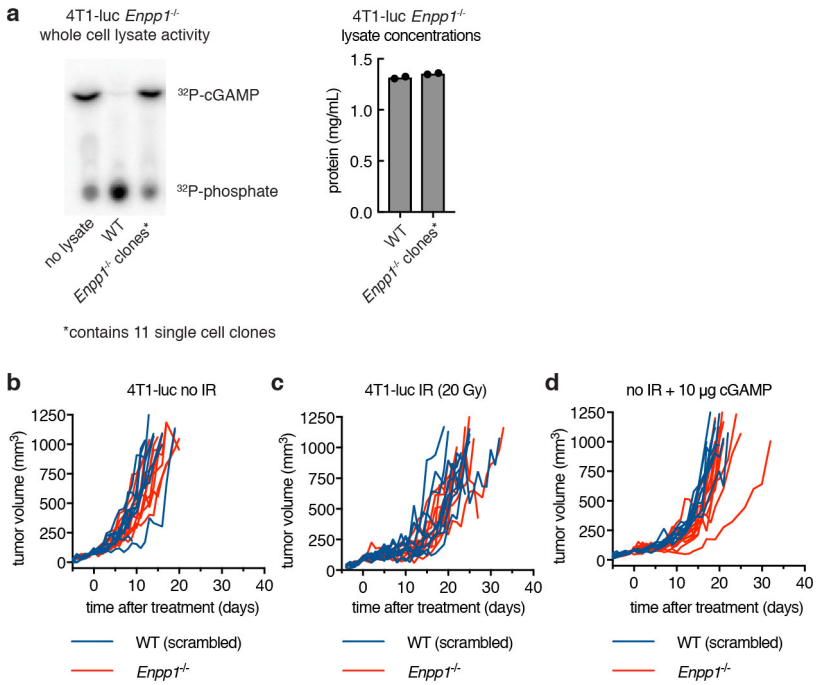

Extended Data Fig. 9 | 4T1-luc *Enpp1*$^{-/-}$ tumor growth. a, Validating *Enpp1*$^{-/-}$ 4T1-luc clones (11 clones were pooled) using the ^{32}P-cGAMP degradation assay (3 day incubation). Lysates were normalized by protein concentrations. Data are from 1 experiment, representative of three independent validations; 2 technical protein concentration replicates are plotted with a bar representing the mean. **b**, Established 4T1-luc WT (harboring scrambled sgRNA) ($n=10$ mice) or *Enpp1*$^{-/-}$ tumors ($n=10$ mice) (100 ± 20 mm^3) were monitored without treatment. Tumor volumes for individual mice are shown. **c**, Established 4T1-luc WT (harboring scrambled sgRNA) ($n=10$ mice) or *Enpp1*$^{-/-}$ tumors ($n=10$ mice) (100 ± 20 mm^3) were treated with IR (20 Gy) and monitored. Tumor volumes for individual mice are shown. **d**, Established 4T1-luc WT (harboring scrambled sgRNA) ($n=9$ mice) or *Enpp1*$^{-/-}$ tumors ($n=9$ mice) (100 ± 20 mm^3) were treated with three intratumoral injections of 10 µg cGAMP on day 2, 4, and 7 and monitored. Tumor volumes for individual mice are shown.

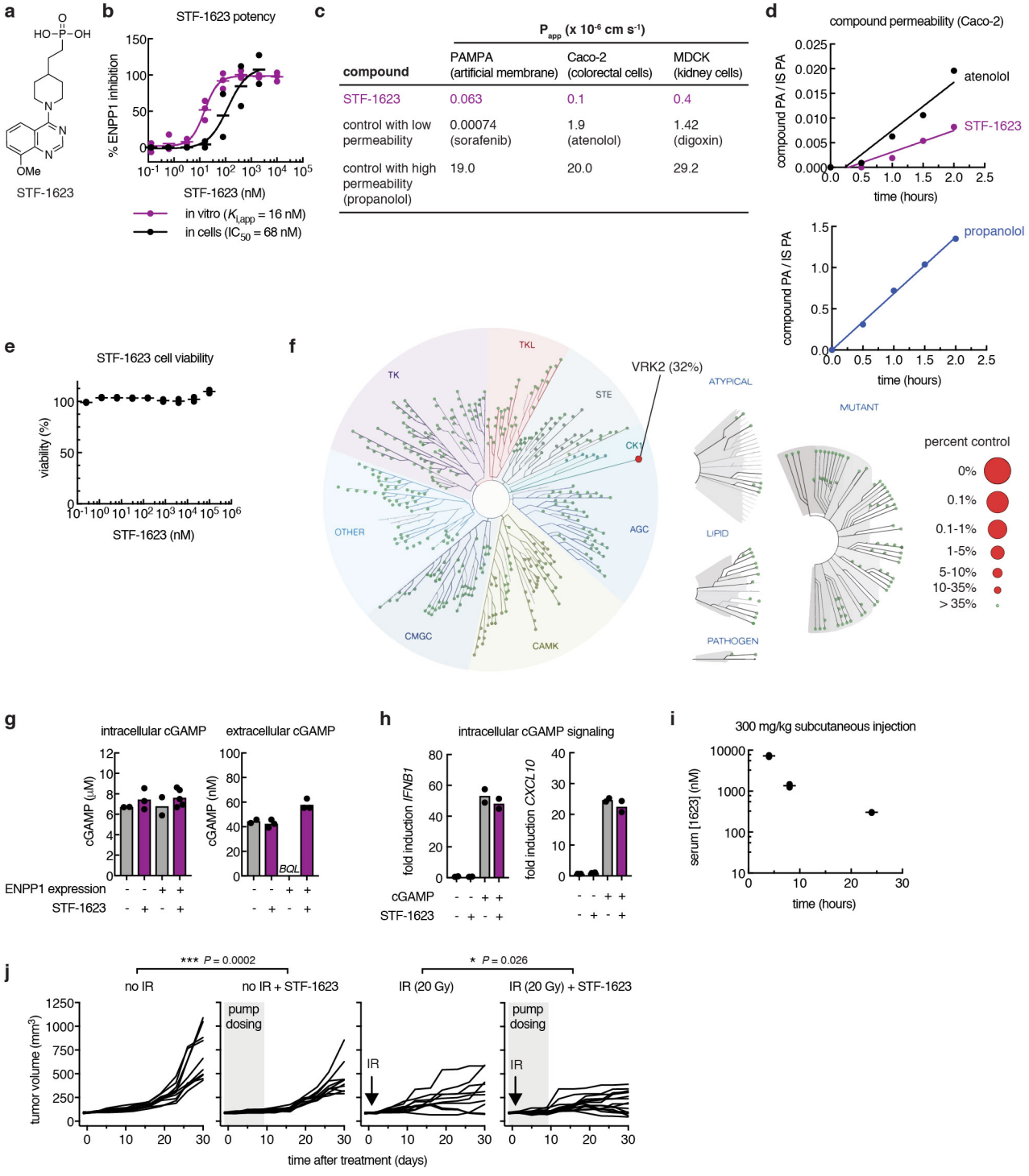

Extended Data Fig. 10 | See next page for caption.

Extended Data Fig. 10 | A systemic ENPP1 inhibitor delays Panc02 tumor growth as a single agent and synergizes with ionizing radiation. **a**, Structure of ENPP1 inhibitor STF-1623. **b**, Inhibition by STF-1623. In vitro (^{32}P-cGAMP TLC assay, pH 7.5, purified mouse ENPP1: $K_{i,app}$ = 16 nM. 3 independent experiments are plotted. In cells (cGAMP export assay, human ENPP1 transfected into 293 T cGAS ENPP1$^{-/-}$ cells): IC_{50} = 68 nM. Data are from 1 experiment; 2 cell culture replicates are plotted. **c**, Mean apparent permeability (P_{app}) for STF-1623 and controls. For PAMPA and MDCK, mean was calculated from 2 cell culture replicates, 1 experiment. For Caco-2, mean was calculated from 2 independent experiments (data for atenolol and propranolol are reproduced from Fig. 3f for comparison). **d**, Permeability of compounds in Caco-2 assay. PA = peak area, IS = internal standard. Compounds were incubated on the apical side of a Caco-2 monolayer for 2 hours. Compound concentration on the basolateral side was monitored by LC-MS/MS. Apparent permeability rates (P_{app}) were calculated from the slope. Data are representative of 2 independent experiments; single points are plotted. **e**, PBMCs were incubated with STF-1623 for 16 h. Data are from one experiment; 2 cell culture replicates are plotted. **f**, Kinome interaction map (468 kinases tested) for STF-1623 depicting kinase inhibition as a percent of control. Data visualized with the TREEspot Software Tool and reprinted with permission from KINOMEscan, a division of DiscoveRx Corporation. ©DiscoveRX Corporation 2010. **g**, Intracellular and extracellular cGAMP concentrations for 293T cGAS ENPP1$^{-/-}$ cells transfected with pcDNA6 (empty or containing human *ENPP1*) and treated ± 2 μM STF-1623 after 24 hours. Data are from 1 experiment; cell culture replicates plotted from left to right are (intracellular) 2, 3, 2, 5 and (extracellular) 2, 3, 2, 3. **h**, PBMCs were electroporated ± 200 nM cGAMP and incubated ± 2 μM STF-1623 for 16 h. *IFNB1* and *CXCL10* mRNA levels were normalized to *ACTB* and fold induction calculated relative to untreated cells. Data are from 1 experiment; 2 cell culture replicates are plotted. **i**, Mice were injected subcutaneously with 300 mg/kg STF-1623 at time 0. At indicated times, the mouse was sacrificed, blood was drawn by cardiac puncture, and serum isolated after clotting. STF-1623 concentrations were measure by LC-MS/MS. Data are from 1 experiment; 2 mice per time point are plotted except for 8 hours, where 3 mice are plotted. **j**, Mice bearing established subcutaneous Panc02 tumors (100 ± 20 mm^3) were implanted with a subcutaneous pump containing STF-1623 (50 mg/kg/day) on day 0 and left untreated or treated with IR (20 Gy) on day 1. No IR: n = 10 mice, no IR + STF-1623: n = 10 mice, IR (20 Gy): n = 10 mice, IR (20 Gy) + STF-1623: n = 15 mice. Pumps were removed on day 8. Tumor volumes for individual mice are shown. *P* value determined by pairwise comparisons using post hoc tests with a Tukey adjustment. In **b** and **g**, cGAMP is measured by LC-MS/MS. *BQL* = below quantification limit. In **b**,**e**,**g**,**h**, and **i**, replicates are plotted individually with a bar representing the mean.

nature research

Corresponding author(s): Lingyin Li

Last updated by author(s): 01/06/2020

Reporting Summary

Nature Research wishes to improve the reproducibility of the work that we publish. This form provides structure for consistency and transparency in reporting. For further information on Nature Research policies, see Authors & Referees and the Editorial Policy Checklist.

Statistics

For all statistical analyses, confirm that the following items are present in the figure legend, table legend, main text, or Methods section.

n/a	Confirmed	
☐	☒	The exact sample size (*n*) for each experimental group/condition, given as a discrete number and unit of measurement
☐	☒	A statement on whether measurements were taken from distinct samples or whether the same sample was measured repeatedly
☐	☒	The statistical test(s) used AND whether they are one- or two-sided *Only common tests should be described solely by name; describe more complex techniques in the Methods section.*
☐	☒	A description of all covariates tested
☐	☒	A description of any assumptions or corrections, such as tests of normality and adjustment for multiple comparisons
☐	☒	A full description of the statistical parameters including central tendency (e.g. means) or other basic estimates (e.g. regression coefficient) AND variation (e.g. standard deviation) or associated estimates of uncertainty (e.g. confidence intervals)
☐	☒	For null hypothesis testing, the test statistic (e.g. *F*, *t*, *r*) with confidence intervals, effect sizes, degrees of freedom and *P* value noted *Give P values as exact values whenever suitable.*
☒	☐	For Bayesian analysis, information on the choice of priors and Markov chain Monte Carlo settings
☐	☒	For hierarchical and complex designs, identification of the appropriate level for tests and full reporting of outcomes
☒	☐	Estimates of effect sizes (e.g. Cohen's *d*, Pearson's *r*), indicating how they were calculated

Our web collection on statistics for biologists contains articles on many of the points above.

Software and code

Policy information about availability of computer code

Data collection	Analyst 1.5, Tecan Spark, Licor Odyssey CLx, Sony SH800S, FlowJo V10, Typhoon 9400 scanner control, 7900HT Fast Real-Time PCR software
Data analysis	Microsoft Excel 365, Graphpad Prism 7.03, FlowJo V10, BD Diva 8, ImageJ, G*Power 3.1, Aura 2.0.1 from Spectral Instruments Imaging, SpectroFlo 2.1, TreeSpot, TraceFinder

For manuscripts utilizing custom algorithms or software that are central to the research but not yet described in published literature, software must be made available to editors/reviewers. We strongly encourage code deposition in a community repository (e.g. GitHub). See the Nature Research guidelines for submitting code & software for further information.

Data

Policy information about availability of data

All manuscripts must include a data availability statement. This statement should provide the following information, where applicable:

- Accession codes, unique identifiers, or web links for publicly available datasets
- A list of figures that have associated raw data
- A description of any restrictions on data availability

The ENPP1 mRNA expression data were derived from the TCGA Research Network: http://cancergenome.nih.gov/. Source Data (numerical and uncropped western blots) and Supplementary Data (independent validations) for Fig. 1–5, and Extended Data Fig. 1–7, 9–10 are provided. All other data that support the findings of this study are available from the corresponding author upon request.

Field-specific reporting

Please select the one below that is the best fit for your research. If you are not sure, read the appropriate sections before making your selection.

☒ Life sciences ☐ Behavioural & social sciences ☐ Ecological, evolutionary & environmental sciences

For a reference copy of the document with all sections, see nature.com/documents/nr-reporting-summary-flat.pdf

Life sciences study design

All studies must disclose on these points even when the disclosure is negative.

Sample size	Treatment of established tumors in mice: power calculations were performed to estimate that cohorts of 9 mice were needed. Calculations were based on a pilot study using a 0.05, 2-sided significance level and power of 0.8, determined by Mann-Whitney U-test. The effect size of 1.9 and power calculations were performed using G*Power 3.1. Mice from different treatment groups were randomly co-housed in each cage to eliminate cage effects. For all other experiments, no statistical method was used to predetermine sample sizes. For FACS analysis of tumors, sample sizes were chosen to be 2-6 mice. For in vitro and cell culture experiments, sample sizes were chosen to be 2-3 biological replicates except in Fig. 2e–g, Fig. 5e, Extended Data Fig. 2b, Extended Data Fig. 3d, and Extended Data Fig. 10d, where titrations or time courses were performed and the sample size was chosen to be 1, with 2 technical replicates.
Data exclusions	No data were excluded from this study.
Replication	Either independent experiments (experiments repeated with identical assay conditions) or independent validations (experiments repeated with similar, but not identical conditions that validate results overall, but not precisely) were performed as indicated in the figure legends. Data from independent validations is shown in the Supplementary Figures as indicated. For data shown in Fig. 1b, f; Fig. 2d; Fig. 3e (in cells assay), f, j; Fig. 4a, b, c (Neuro-2a, MDA-MB-231, HeLa); Extended Data Fig. 3f, Extended Data Fig. 4a, e; and Extended Data Fig. 10b (in cells assay), d–f, the experiment was performed once. The result was supported by orthogonal experiments in other panels, as indicated in figure legends.
Randomization	Mice from different treatment groups were randomly co-housed in each cage to eliminate cage effects.
Blinding	The experimenter was blinded to group allocation and data analysis for mouse experiments.

Reporting for specific materials, systems and methods

We require information from authors about some types of materials, experimental systems and methods used in many studies. Here, indicate whether each material, system or method listed is relevant to your study. If you are not sure if a list item applies to your research, read the appropriate section before selecting a response.

Materials & experimental systems

n/a	Involved in the study
☐	☒ Antibodies
☐	☒ Eukaryotic cell lines
☒	☐ Palaeontology
☐	☒ Animals and other organisms
☒	☐ Human research participants
☒	☐ Clinical data

Methods

n/a	Involved in the study
☒	☐ ChIP-seq
☐	☒ Flow cytometry
☒	☐ MRI-based neuroimaging

Antibodies

Antibodies used	rabbit anti-cGAS (15102S Cell Signaling, clone D1D3G, 1:1,000) rabbit anti-mouse cGAS (31659S Cell Signaling, clone D2O8O 1:1,000), mouse anti-tubulin (3873S Cell Signaling, clone DM1A, 1:2,000), rabbit anti-STING (13647S Cell Signaling, clone D2P2F, 1:1,000),), rabbit anti-phospho-IRF3 (4D4G Cell Signaling, 1:1,000), rabbit anti-IRF3 (D83B9 Cell Signaling, 1:1,000), IRDye 800CW goat anti-rabbit (926-32211 LI-COR, 1:15,000), IRDye 680RD goat anti-mouse (926-68070 LI-COR, 1:15,000). TruStain fcX (101320 BioLegend, clone 93, 1:100), CD8α-AF594 (100758 BioLegend, clone 53-6.7, 1:200), CD11c-PE (117308 BioLegend, clone N418, 1:200), CD45-AF700 (103128 BioLegend, clone 30-F11, 1:800), CD45-BV650 (103151 BioLegend, clone 30-F11, 1:100), CD62L-BV785 (104440 BioLegend, clone MEL-14, 1:200), F4/80-APC (123116 BioLegend, clone BM8, 1:200), Granzyme B-AF647 (515406 BioLegend, clone GB11, 1:100), I-A/I-E-FITC (107606 Biolegend, clone M5/114.15.2, 1:800), CD3ε-PerCP-eF710 (46-0033-82 eBioscience, clone eBio500A2, 1:200), CD25-eF450 (48-0251-82 eBioscience, PC61.5, 1:200), CD103-BUV395 (740238 BD Biosciences, clone M290, 1:400)
Validation	rabbit anti-cGAS: validated on NK-92, NCI-H460, MCF7, THP-1, and U-937 cells (Cell Signaling) rabbit anti-mouse cGAS: validated on 3T3, Neuro-2a, and C2C12 cells (Cell Signaling) mouse anti-tubulin: validated on HeLa and COS-7 cells (Cell Signaling) rabbit anti-STING: validated on THP-1, HT-29, HaCaT, HL-60, A20, BaF3, C2C12, and EL4 cells (Cell Signaling)

rabbit anti-phospho-IRF3: validated on HT29 and THP-1 cells, control or plpC-transfected (1 hour) (Cell Signaling)
rabbit anti-IRF3: validated on HeLa, THP-1, U937, Jurkat, NIH/3T#, MEF, Raw 264.7, C6, KNRK, and H-4-II-E cells (Cell Signaling)
CD8α-AF594: validated on mouse lymph nodes (BioLegend)
CD11c-PE: validated on mouse splenocytes (BioLegend)
CD45-AF700: validated on mouse splenocytes (BioLegend)
CD45-BV650: validated on mouse splenocytes (BioLegend)
CD62L-BV785: validated on mouse splenocytes (BioLegend)
F4/80-APC: validated on thioglycolate-elicited BALB/c mouse peritoneal macrophages (BioLegend)
Granzyme B-AF647: validated on human peripheral blood lymphocytes and mouse splenocytes stimulated with plate-bound anti-mouse TCR-beta (BioLegend)
I-A/I-E-FITC: validated on mouse splenocytes (BioLegend)
CD3ε-PerCP-eF710: validated on mouse splenocytes (eBioscience)
CD25-eF450: validated on mouse splenocytes (eBioscience)
CD103-BUV395: "verification testing has not been performed on all conjugate lots" (BD Biosciences)

Eukaryotic cell lines

Policy information about cell lines

Cell line source(s)	293T, NMuMG, MDA-MB-231, HeLa, MCF-7, and Neuro-2a were procured from ATCC, Panc02 was procured from the DTP/DCTD/NCI Tumor Repository, E0771 was procured from CH3 BioSystems, 4T1-luciferase (4T1-luc) was a gift from Dr. Christopher Contag, and HEK293S GnT1- expressing secreted mENPP1 was a gift from Dr. Osamu Nureki.
Authentication	None of the cell lines used were authenticated.
Mycoplasma contamination	All cell lines tested negative for mycoplasma.
Commonly misidentified lines (See ICLAC register)	No commonly misidentified cell lines were used in this study.

Animals and other organisms

Policy information about studies involving animals; ARRIVE guidelines recommended for reporting animal research

Laboratory animals	Five- to nine-week-old female BALB/c mice (Jackson Laboratories) and five- to nine-week-old female WT, cGAS-/-, STING-/-, or ENPP1-/- C57BL/6J mice (Jackson Laboratories) were used in this study.
Wild animals	This study did not involve wild animals.
Field-collected samples	This study did not involve samples collected from the field.
Ethics oversight	All animal procedures were approved by the Stanford University Administrative Panel on Laboratory Animal Care (APLAC).

Note that full information on the approval of the study protocol must also be provided in the manuscript.

Flow Cytometry

Plots

Confirm that:

☒ The axis labels state the marker and fluorochrome used (e.g. CD4-FITC).

☒ The axis scales are clearly visible. Include numbers along axes only for bottom left plot of group (a 'group' is an analysis of identical markers).

☒ All plots are contour plots with outliers or pseudocolor plots.

☒ A numerical value for number of cells or percentage (with statistics) is provided.

Methodology

Sample preparation	Tumors were extracted and incubated in RPMI + 10% FBS with 20 mg/mL DNase I type IV (Sigma-Aldrich) and 1 mg/mL Collagenase from Clostridium histolyticum (Sigma-Aldrich) at 37 °C for 30 min. Tumors were passed through a 100 mm cell strainer (Sigma-Aldrich) and red blood cells were lysed using red blood cell lysis buffer (155 mM NH4Cl, 12 mM NaHCO3, 0.1 mM EDTA) for 5 min at room temperature. Cells were stained with Live/Dead fixable near-IR dead cell staining kit (Thermo Fisher Scientific, 1:1000 in accordance with the manufacturer's description), Fc-blocked for 10 min using TruStain fcX (101320 BioLegend, clone 93, 1:100) and subsequently antibody-stained with CD8α-AF594 (100758 BioLegend, clone 53-6.7, 1:200), CD11c-PE (117308 BioLegend, clone N418, 1:200), CD45-AF700 (103128 BioLegend, clone 30-F11, 1:800) or BV650 (103151 BioLegend, clone 30-F11, 1:100), CD62L-BV785 (104440 BioLegend, clone MEL-14, 1:200), F4/80-APC (123116 BioLegend, clone BM8, 1:200), Granzyme B-AF647 (515406 BioLegend, clone GB11, 1:100), I-A/I-E-FITC (107606 Biolegend, clone M5/114.15.2, 1:800), CD3ε-PerCP-eF710 (46-0033-82 eBioscience, clone eBio500A2, 1:200), CD25-eF450 (48-0251-82 eBioscience, PC61.5, 1:200), and CD103-BUV395 (740238 BD Biosciences, clone M290, 1:400). Caspase activity was detected after red blood cell lysis using the FAM-FLICA Poly Caspase Assay Kit (ImmunoChemistry

Technologies) according to the manufacturer's description.

Instrument

SH800S cell sorter (Sony), Aurora (Cytek), or LSR II (BD Biosciences).

Software

Data was collected using BD Diva, Sony SH800S cell sorter software or Cytek SpectroFlo and analyzed using FlowJo V10 software (Treestar) and Prism 7.04 software (Graphpad) for statistical analysis and statistical significance was assessed using the unpaired t test with Welch's correction.

Cell population abundance

No cell sorting was performed.

Gating strategy

APC / DC analysis: FSC-A / SSC-A: the gate was set to exclude cellular debris (FSC-A low events); FSC-W / SSC-A: the gate was set to include the singlet population, excluding FSC-W high doublets; Live/Dead-Near-IR / SSC-A: the gate was set to include the living cells (Live/Dead-Near-IR low) and to exclude dead cells (Live/Dead-Near-IR high population); CD45-AF700 / SSC-A: The gate was set to include the CD45+ lymphocytes, excluding all negative cells; MHC II-FITC / SSC-A: The gate was set to include the MHC II+ APCs, excluding all other lymphocytes; CD11c-PE / SSC-A: The gate was set to include the CD11c+ DCs, excluding CD11c- APCs; CD103-BUV395 / SSC-A: The gate was set to include the CD103+ DCs out of the CD11c+ gate previously described to include the cross-presenting cDC1 population; F4/80-APC / SSC-A: The gate was set to include the F4/80 high macrophages, excluding F4/80 intermediate to low APCs.
Live-Dead analysis: FSC-A / SSC-A: the gate was set to include cells and debris; CD45-AF700 / SSC-A: Two gates were set to distinguish between the CD45+ lymphocytes and the CD45- tumor and stromal cells - from both of these, geometric means of the Live/Dead-Near-IR stain and of the Caspase stain were analyzed.
T-cell activation analysis: FSC-A / SSC-A: the gate was set to exclude cellular debris (FSC-A low events); FSC-W / SSC-A: the gate was set to include the singlet population, excluding FSC-W high doublets; Live/Dead-Near-IR / SSC-A: the gate was set to include the living cells (Live/Dead-Near-IR low) and to exclude dead cells (Live/Dead-Near-IR high population); CD45-BV650 / SSC-A: The gate was set to include the CD45+ lymphocytes, excluding all negative cells; CD3-PerCP-eF710 / SSC-A: The gate was set to include the CD3+ T-cells, excluding all non-T-cells in the lymphocyte gate; CD8-AF594 / SSC-A: The gate was set to include the CD8+ cytotoxic T-cells, excluding CD8- T-cells; Out of this subset, geometric means for CD25-eF450, CD62L-BV785, and Granzyme B-AF647 were analyzed.

☒ Tick this box to confirm that a figure exemplifying the gating strategy is provided in the Supplementary Information.